UNIVERSIDADE ESTADUAL DE CAMPINAS
INSTITUTO DE QUÍMICA

MURILO IZIDORO SANTOS

3D PRINTED POLY(ACRYLIC ACID)-F127-CELLULOSE NANOCRYSTAL HYBRID HYDROGELS FOR NITRIC OXIDE DELIVERY

HIDROGÉIS IMPRESSOS DE POLI(ÁCIDO ACRÍLICO)-F127-NANOCRISTAIS DE CELULOSE PARA ENTREGA DE ÓXIDO NÍTRICO

CAMPINAS
2020

MURILO IZIDORO SANTOS

3D PRINTED POLY(ACRYLIC ACID)-F127-CELLULOSE NANOCRYSTAL HYBRID HYDROGELS FOR NITRIC OXIDE DELIVERY

HIDROGÉIS HÍBRIDOS IMPRESSOS DE POLI(ÁCIDO ACRÍLICO)-F127-NANOCRISTAIS DE CELULOSE PARA ENTREGA DE ÓXIDO NÍTRICO

Dissertação de Mestrado apresentada ao Instituto de Química da Universidade Estadual de Campinas como parte dos requisitos exigidos para a obtenção do título de Mestre em Química na área de Físico-Química

Master's Dissertation presented to the Institute of Chemistry of the University of Campinas as part of the requirements to obtain the title of Master in Chemistry in the area of Physical Chemistry.

Orientador: Prof. Dr. Marcelo Ganzarolli de Oliveira
Co-orientadora: Profa. Dra. Maria do Carmo Gonçalves

O arquivo digital corresponde à versão final da Dissertação defendida pelo aluno Murilo Izidoro Santos e orientada pelo Prof. Dr. Marcelo Ganzarolli de Oliveira.

CAMPINAS
2020

Ficha catalográfica
Universidade Estadual de Campinas
Biblioteca do Instituto de Química
Simone Luiz Alves - CRB 8/9094

Sa59t

Santos, Murilo Izidoro, 1993-
3D printed poly(acrylic acid)-F127-cellulose nanocrystal hydbrid hydrogels for nitric oxide delivery / Murilo Izidoro Santos. – Campinas, SP : [s.n.], 2020.

Orientador: Marcelo Ganzarolli de Oliveira.
Coorientador: Maria do Carmo Gonçalves.
Dissertação (mestrado) – Universidade Estadual de Campinas, Instituto de Química.

1. Impressão tridimensional. 2. Hidrogel. 3. Fotopolimerização. 4. Óxido nítrico. I. Oliveira, Marcelo Ganzarolli de, 1959-. II. Gonçalves, Maria do Carmo, 1957-. III. Universidade Estadual de Campinas. Instituto de Química. IV. Título.

Informações para Biblioteca Digital

Título em outro idioma: Hidrogéis impressos de poli(ácido acrílico)-F127-nanocristais de celulose para entrega de óxido nítrico
Palavras-chave em inglês:
Printing, three-dimensional
Hydrogel
Photopolymerization
Nitric oxide
Área de concentração: Físico-Química
Titulação: Mestre em Química na área de Físico-Química
Banca examinadora:
Marcelo Ganzarolli de Oliveira [Orientador]
Camila Alves de Rezende
Amedea Barozzi Seabra
Data de defesa: 31-03-2020
Programa de Pós-Graduação: Química

Identificação e informações acadêmicas do(a) aluno(a)
- ORCID do autor: http://orcid.org/0000-0001-7639-6409
- Currículo Lattes do autor: http://lattes.cnpq.br/2807723317358815

BANCA EXAMINADORA

Prof. Dr. Marcelo Ganzarolli de Oliveira (Orientador)

Profa. Dra. Camila Alves de Rezende (IQ-UNICAMP)

Profa. Dra. Amedea Barozzi Seabra (CCNH - UFABC)

A Ata da defesa, assinada pelos membros da Comissão Examinadora, consta no SIGA/Sistema de Fluxo de Dissertação/Tese e na Secretaria do Programa da Unidade.

Este exemplar corresponde à redação final da Dissertação de Mestrado defendida pelo aluno **MURILO IZIDORO SANTOS**, aprovada pela Comissão Julgadora em 31 de março de 2020.

Window on utopia (Ventana sobre la utopia)

"She is on the horizon, says Fernando Birri.
I walk two steps, she moves two steps away.
I walk ten steps and the horizon runs ten steps further.
As much as I walk, I will never reach her.
For what does utopia serve? It serves for this:to walk."
- Eduardo Galeano (1940-2015), Las Palabras Andantes, 1993

Acknowledgements

Firstly, I would like to thank my supervisor, Professor Marcelo Ganzarolli, for accepting me as a student, for the supervision and most of all, for igniting my flame of creativity. Professor Maria do Carmo is thanked not only for being my co-supervisor, but also for being my example of professional. I am especially grateful for all the nice and motivating talks we had; whenever I talk to you, I feel relief.

Thanks to Laura, for all the assistance with the analyses and the exchange of ideas. I also owe thanks to you for the valuable personal and professional advice. Because of you, I am certain that there is still hope for Brazil, at least for its science.

The National Research Council (CNPq, no. 130619/2018-3) is acknowledged for the financial support.

This study was also financed in part by the São Paulo Research Foundation (FAPESP, no. 2016/02414-5).

Thanks to the infrastructure provided by the Institute of Chemistry (IQ) and UNICAMP.

The security staff deserves to be remembered, especially Nestor and Cristiano, who accompanied me during all these years in the IQ, sometimes even after 10 PM.

I would also like to thank the lab technicians: Monique and Charles for making my life easier; To Hugo, for training me on SEM; to Fabiana, for the support with thermal and mechanical analyses of the hydrogels, and to Ricardo and Karen for the help with UPLC.

Thanks to Marcelo Farias and Antônio Borges, from the Brazilian Nanotechnology National Laboratory (LNNano), Campinas, SP, for the great support with sample preparation and insights into cryo-TEM. Also, to Dr. Mônica Helena Monteiro do Nascimento, Felipe Nogueira Ambrosio, Prof. Christiane Bertachini Lombello and Prof. Amedea Barozzi Seabra from the ABC Federal University (UFABC), Santo André, SP, for the preliminary evaluation of cytotoxicity of the materials.

I could not forget to say thanks to all the members of the Nitric Oxide Biomaterials Group: Matheus, Giovanna, Daniele, Yasmim and Marina, for all the memorable moments we had. Of course, I owe special thanks to Mateus Peres, who had the misfortune to work with me during his scientific initiation.

There are still very special people that must be remembered here:

To my parents, Deonice and Eduardo, who brought me into this world and always provided the best they could for their children, even in hard times. I owe you eternal gratitude.

To my sisters, Marina and Meire, for their example, obstinacy, and to always believe in my capacities, even when I did not trust myself.

And, of course, to Larissa, who is more than just a girlfriend or a partner, is someone who makes my life far more interesting and joyful… and colorful, and tasty!

To my friends: Agnes, Chárbel, Douglas, Letícia, Ian, João Paulo, Mateus(in), Eupídio, Elisa, Camilla, Victor, Thiago, Guilherme (Sumido). You made me who I am too. For that, no money can pay.

I would like to say that I praise life in every form and color, because it gave me the opportunity to share wonderful experiences with all the people that I mentioned in these lines. I hope we can write a lot more lines together.

MURILO I. SANTOS

Resumo

Hidrogéis têm sido amplamente propostos como plataformas de liberação de óxido nítrico (NO) devido à comprovada ação cicatrizante do NO, fazendo-os ótimos candidatos para a produção de *scaffolds* em engenharia de tecidos. Contudo, tais aplicações requerem formatos complexos e detalhados, muitas vezes não atingidos por simples moldagem. Este inconveniente pode ser contornado pela manufatura aditiva, popularmente chamada de impressão 3D, ainda pouco explorada com sistemas desenvolvidos para a entrega de NO. Este trabalho mostra o desenvolvimento de hidrogéis semi-interpenetrados baseados em poli(ácido acrílico) (PAA), Pluronic F127 (F127) e nanocristais de celulose (CNCs) (PAA/F127/CNC) para a liberação controlada de NO via Processamento Digital de Luz (DLP). As formulações para impressão dos hidrogéis foram desenvolvidas com o auxílio de metodologias de planejamento de experimentos (DOE), que mostraram grande contribuição de efeitos composicionais nas propriedades mecânicas dos materiais testados. Adicionalmente, hidrogéis contendo até 1% m/m de CNCs foram impressos com sucesso, formando estruturas com menos de 200 µm de espessura. Os hidrogéis PAA/F127/CNC preservaram estruturas micelares características do F127 contidas nos materiais. Além disso, os hidrogéis impressos apresentaram morfologia densa, sem evidências de separação de camadas de impressão. Porém, agregados de CNCs foram observados quando concentrações acima de 0.25 m/m% CNCs foram empregadas e podem estar relacionados a falhas nas propriedades mecânicas destes hidrogéis. A adição de CNCs revelou ainda efeito modulador na cinética de intumescimento e provocou aumento nas taxas de liberação de NO dos hidrogéis PAA/F127/CNC. Testes preliminares de citotoxicidade mostraram viabilidade celular aceitável quando hidrogéis impressos foram lavados em tampão PBS, tornando hidrogéis PAA/F127/CNC candidatos a pesquisas mais aprofundadas com biomateriais destinados à entrega de NO.

Abstract

Hydrogels have been widely proposed as platforms for nitric oxide (NO) release due to the proven wound healing activity of NO, making them good candidates to produce scaffolds in tissue engineering. However, such applications require complex and detailed shapes, frequently not achievable by simple molding. This drawback can be overcome by additive manufacturing, popularly called 3D printing, which is still scarcely explored in systems designed to NO delivery. This work shows the development of semi-interpenetrating hydrogels based on poly(acrylic acid) (PAA), Pluronic F127 (F127) and cellulose nanocrystals (CNCs) – PAA/F127/CNC via Digital Light Processing (DLP) for NO controlled release. Hydrogel printable formulations were developed with the help of design of experiment (DOE) tools, which showed high contribution of compositional effects in mechanical properties of the tested materials. Additionally, hydrogels containing up to 1 wt% CNCs were successfully printed, producing less than 200 μm-wide constructs. PAA/F127/CNC hydrogels preserved the characteristic F127 micellar structures enclosed in the materials. Moreover, printed hydrogels displayed dense morphologies, without evidence of layer tearing. However, CNC aggregates were observed when concentrations higher than 0.25 wt% CNCs were employed and may be related to failure in mechanical properties. Still, CNC introduction revealed a modulating effect in swelling kinetics and increased NO release rates. Preliminary citotoxicity tests showed acceptable cell viability when printed hydrogels were washed in PBS solution, making the PAA/F127/CNC hydrogels candidates for further research in NO donor biomaterials.

List of Figures

List of Tables

List of Abbreviations

2D	Two-dimensional
3D	Three-dimensional
AA	Acrylic Acid
ANOVA	Analysis of Variance
ATR	Atenuated Total Reflectance
CAD	Computer-aided Design
CNC	Cellulose Nanocrystals
Cryo-TEM	Cryogenic Transmission Electron Microscopy
CT	Computed Tomography
DLP	Digital Light Processing
DMD	Digital Micromirror Device
DOE	Design of Experiments
F127	Pluronic® F127
FCC	Face-Centered Cubic
FDA	Food and Drug Administration
FFT	Fast Fourier transform
FTIR	Infrared Vibrational Spectroscopy
G'	Dynamic storage modulus
GSH	Glutathione reduced
GSNO	S-nitrosoglutathione
IPN	Full Interpenetrating Network
IUPAC	International Union for Pure and Applied Chemistry
LED	Light Emitting Diode
MBA	N,N'-methylenebisacrylamide
MEHQ	4-Methoxyphenol
NO	Nitric Oxide
NOA	Nitric Oxide Analyzer
PAA	Poly(acrylic acid)
PBS	Phosphate Buffered Saline
PEO	Poly(ethylene oxide)
PPO	Poly(propylene oxide)
PTFE	Polytetrafluorethylene, Teflon®
PVA	Poly(vinyl alcohol)
SAXS	Small-Angle X-Ray Scattering
SEM	Scanning Electron Microscopy

Semi-IPN	Semi-Interpenetrating Network
TEM	Transmission Electron Microscopy
TMA	Thermomechanical Analysis
UV	Ultraviolet
YM	Young's Modulus

Contents

Introduction

Hydrogels

According to the IUPAC, gels are materials formed by colloidal or polymeric matrices expanded by a fluid. When expansion is driven by water, a hydrogel is obtained.[1]

Hydrogels are formed by tridimensional crosslinked polymers with hydrophilic character, capable to retain up to 1000 times their dry weight in water.[2,3] Water retention, flexibility, and nutrient permeability in hydrogels share similarities to living tissues and make them attractive for biological applications,[4] such as wound dressings, contact lenses and tissue scaffolds.

Hydrogels are versatile materials, due to the diversity in synthetic approaches and existent hydrophilic polymers. The junction points between the polymer chains are called crosslinks and can be based on non-covalent bonds, resulting in physically crosslinked hydrogels. Materials such as gelatins, the popular slimes obtained by tetraborate (borax) and poly(vinyl alcohol) (PVA) crosslinking[5] and calcium alginate gels[6] are classic examples of physical hydrogels. Alternatively, the polymer chains can be crosslinked by chemical reactions, such as thiol-ene coupling[7] or free-radical polymerization of vinyl monomers.[8–10] Chemical crosslinking has advantages over simple physical association, since the permanent junctions enable a better control over composition and physical properties, what broadens the possible uses of the hydrogels.

The so called “smart hydrogels” are susceptible to changes in the swelling rates driven by external stimuli, *e.g.* temperature, pressure, ligand-specific interactions, pH, *etc.*[11] and have drawn attention of material scientists, being promising strategies to obtain smart medical devices.

Poly(acrylic acid) hydrogels

Poly(acrylic acid) (PAA) is considered a model of pH-responsive polymer, due to the pendant carboxyl groups in the polymer backbone. These functional groups confer a pronounced hydrophilic character to PAA, since they can establish hydrogen bonds with water molecules. When pH is greater than the acrylic acid pKa (pH = 4.75),[12] carboxyl

deprotonation leads to a polyanionic structure, with higher osmotic pressure and intense water uptake. In such a condition, PAA is considered a superabsorbent polymer (**Fig. 1**)

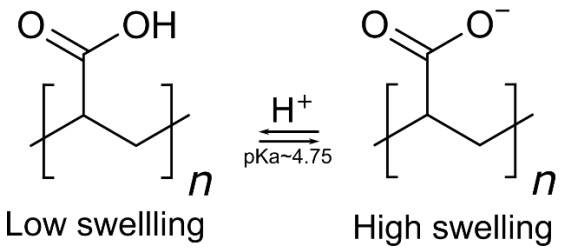

Figure 1. Representation of the PAA ionization equilibrium.

The superabsorbent capacity of PAA is extensively used in products from diapers to medical patches for fluid absorption. Additionally, non-crosslinked PAA (carbomers) are used in cosmetic formulations as dispersing agents, emulsifiers and rheology modifiers.[13]

PAA can be crosslinked with small amounts of polyfunctional monomers (crosslinkers). The resulting PAA hydrogels exhibit good biocompatibility.[14] However, the brittleness of PAA hydrogel pieces is notable and, in most cases, PAA is blended or copolymerized with other polymers, resulting in multicomponent hydrogels.[15–17]

Multicomponent Hydrogels

Recent advances in hydrogels for tissue scaffolds and drug delivery applications focus on hybrid hydrogels, in which synthetic and natural polymers, or even nanomaterials[18] are combined to mimic properties from the host environment and to tune the drug release kinetics. Polymers can be combined via copolymerization or by means of multicomponent networks: full interpenetrating networks (IPN) or semi-interpenetrating networks (semi-IPN). The IPN networks consist of two or more intertwined crosslinked networks, without covalent bonds between them. In thesis, it is impossible to separate the polymers in full IPN networks, except by breaking chemical bonds. On the other hand, semi-IPN networks contain non-crosslinked polymers (linear or branched) dispersed into a crosslinked network and in thesis, their separation does not require breaking of covalent bonds[1] (**Fig. 2**).

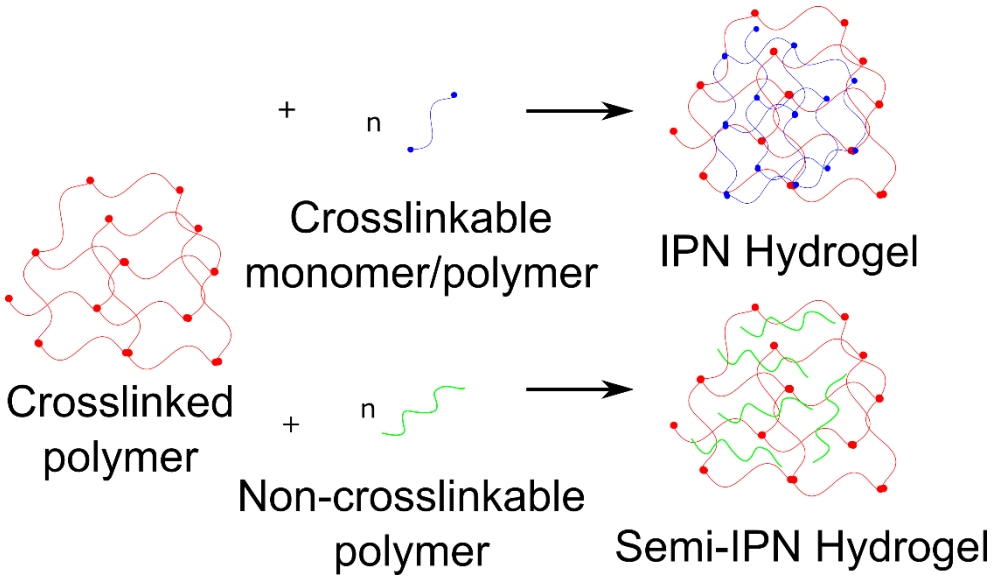

Figure 2. Schematic representation of the components involved in the synthesis of interpenetrating (IPN) and semi-interpenetrating (semi-IPN) networks.

Pluronic® F127

The production of multicomponent hydrogels is a common strategy to improve PAA mechanical properties maintaining pH-responsiveness.[19–21] Baskan and coworkers[10] reported the synthesis of IPN hydrogels by thermoinduced copolymerization of acrylic acid (AA) and N,N'-methylenebisacrylamide (MBA), in the presence of 20 w/v% Pluronic F127 (PEO_{100}-PEO_{65}-PEO_{100} - F127). The resulting hydrogels showed increased compression strength and toughness, compared to pure PAA, as well as thermo-responsiveness, derived from the F127.

The polymer class known as poloxamers (trade name: Pluronics – BASF) is represented by triblock polyol copolymers made up of a central hydrophobic poly(propylene oxide) block flanked by two hydrophilic poly(ethylene oxide) blocks, forming a symmetrical PEO_x-PPO_y-PEO_x structure, which confers them an amphiphilic character and surface activity, in resemblance to long-chain polar surfactants.[22]

F127 is a well-studied poloxamer and its amphiphilicity leads to self-assembling in micelle structures. This phenomenon relates to hydrophobic interactions and dehydration of PPO central blocks.[23,24] The change in hydrophilicity of PPO and PEO blocks induced by temperature, as well as the growing repulsive interactions between micelles, driven by the increase in polymer concentration, promote sol-gel transitions, characterized by a long-range ordering of micelles, the so-called liquid crystals[25] (**Fig. 3**).

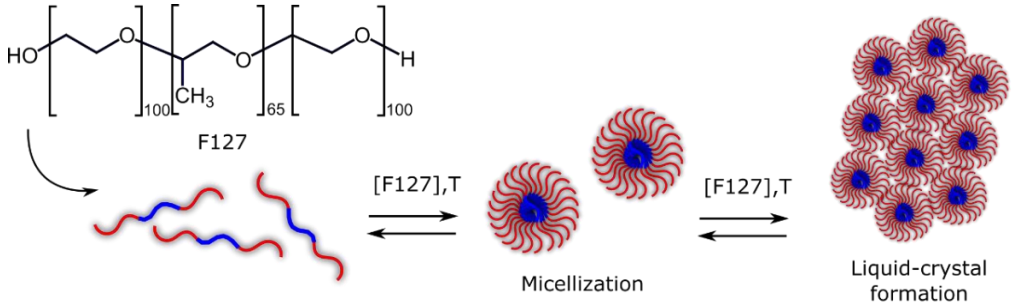

Figure 3. Schematic representation of the reversible micellization and liquid crystal formation in aqueous F127 solutions.

The micellization and gelation processes in Pluronics are closely related to the relative size of PEO and PPO blocks. At room temperature, aqueous solutions of F68 (PEO_{80}-PPO_{30}-PEO_{80}) gel at concentrations above 50 w/v%.[23,26] In similar conditions, F127 (PEO_{100}-PEO_{65}-PEO_{100}) shows the lowest gelation onset concentration among the Pluronics (20 w/v%),[23,24] which is an appealing feature for medical applications.

Due to its low toxicity,[27] F127 has been studied in medical formulations as a dispersing agent for hydrophobic drugs.[28] Additionally, the Food and Drug Administration (FDA) approved a formulation for temporary endovascular occlusion of blood vessels containing 20 wt/vol% F127,[29] thus stimulating a search for new medical uses for this polymer.

Recently, our research group produced hydrogels comprised of PAA crosslinked by MBA in the presence of F127 to obtain supramolecular hydrogels containing packed F127 micelles. The presence of such structures after thermally induced photocrosslinking was capable to control hydrogel swelling rates and to modulate the kinetics of nitric oxide (NO) release for therapeutic applications.[30]

Considering the potential structure directing actions of F127, due to micelle self-assembling, it is expected that these structures may induce structural changes in semi-IPN hydrogels capable to improve drug release kinetics. Moreover, the hydroxyl chain-ends in F127 may provide multiple anchoring points between the crosslinked PAA network and the micellar structures. Summing up all these features, this work proposes to use semi-IPN constructs, made up of PAA and F127, as a framework to develop hybrid hydrogels for drug delivery applications.

Cellulose Nanocrystals (CNCs)

Lignocellulosic materials have been widely used to produce hydrogels and composite materials, owing to their distinctive features such as renewability, availability, biocompatibility, biodegradability, low density and the addition of value to biomass.[31,32] Among these materials, great attention is focused on cellulose nanocrystals (CNCs), which are essentially rod-shaped nanostructures with a 3 – 10 nm diameter and length between 100 – 500 nm, consisting of cellulose with high degrees of crystallinity.[33,34] CNCs are obtained from cellulose contained in plant cells, bacteria, fungi and even animals (tunicates).[33]

Cellulose chains consist in D-glucopyranose units bound by β-1,4-glycosidic linkages and are found in nature as semi-crystalline fibers. Upon exposure to strong acids, glycosidic linkages in amorphous domains are preferentially cleaved and the crystalline domains are released. Generally, hydrolysis of cellulosic fibers is performed by sulfuric acid and introduces anionic sulfate half-ester groups on the CNC surface. Further mechanical processing or ultrasonication produces the CNCs.[33] Nowadays, CNCs obtained from different sources and chemical treatments are commercially available, such as the sulfate half-ester CNCs produced at the University of Maine employed in this work, shown in **Fig. 4**.

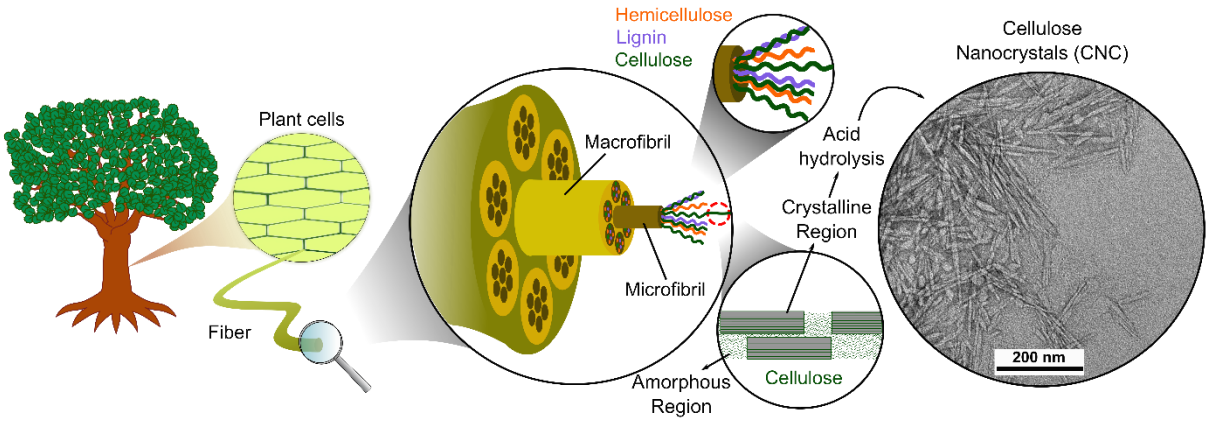

Figure 4. Schematic representation of the hierarchical structure of cellulosic fibers, location of CNCs in the microfibrils and TEM micrograph of the commercial CNCs used in this work. Scheme adapted from Martin-Martinez et al.[35]

CNCs show impressive mechanical properties, being capable to bear longitudinal stresses of *ca.* 8 GPa, with axial stiffness about 150 GPa, along with low density (*ca.* 1.6 g

cm^{-3})[32] and high surface area (400 – 500 $m^2 g^{-1}$)[36]. All the above cited properties make CNCs promising reinforcement agents in composite materials.

Composite hydrogels containing CNCs are commonly prepared by simple dispersion of CNCs into a monomer precursor mixture, followed by free-radical polymerization, resulting in semi-IPN networks.[37,38] Lim and coworkers[20] produced PAA-based semi-IPN networks in the presence of CNCs and reported increases in the hydrogel storage moduli according to CNC mass proportion.

Furthermore, above a certain threshold concentration (usually *ca.* 10 wt/wt%) CNCs can self-assemble into ordered, nematic phases.[39] Hydrogel crosslinking in the presence of such structures can lead to macroscopic percolation networks, which are frequently associated with mechanical reinforcement of these hydrogels. These networks show better dissipation of energy during deformation, due to the transient physical interactions between nanocrystals.[40] Despite the advantages of percolated CNC networks, the hydrogels containing physically entrapped CNCs are usually produced under low CNC concentrations (0 – 6 wt/wt% based on swollen hydrogel weight),[34] probably due to a tendency of high-concentrated CNC samples to aggregate in polymeric solutions. Consequently, crosslinking and mechanical properties are imparted.[32,41] The presence of CNCs in composite materials can also contribute to improve barrier properties, since CNCs can obstruct pores and extend diffusion pathways, together with a decrease in matrix elasticity, caused by hydrogen bonding between CNCs and the crosslinked polymer.[42] Consequently, CNCs can be used as a strategy to modulate the kinetics of water swelling.

This work aims at producing hybrid hydrogels based primarily on PAA and F127 containing CNCs as a filler additive. Considering the advantages of CNCs, such as their hydrophilicity and intrinsic mechanical strength, CNCs could act not only improving hydrogel mechanical properties, but also tuning drug release, which is intensely connected to swelling kinetics.

3D Printing (Additive Manufacturing)

The manufacturing processes based on simple molding and casting limit the possible uses of hydrogels when complex geometries are required. After Charles Hull's Stereolithography apparatus in the late 80's,[43] the rise and popularization of additive

manufacturing techniques, commonly called 3D printing, has circumvented these limitations and engaged scientists to produce customer-tailored medical devices that are rapidly evolving to cell-laden hydrogel constructs, intended to print tissues and even whole organs by a process known as bioprinting.[44]

All 3D printing processes share a common chain of events,[45] starting from the modelling by computer-aided design (CAD) or data obtained by computed tomography (CT) scan. Then, the 3D model is digitally processed in form of printing layers, in a process called slicing and sent to the printer. The fabrication step occurs in a layer-by-layer fashion and afterwards the construct can pass through post-processing, in order to remove printing supports and to apply thermal or post-curing treatments, resulting in 3D objects (**Fig. 5**).

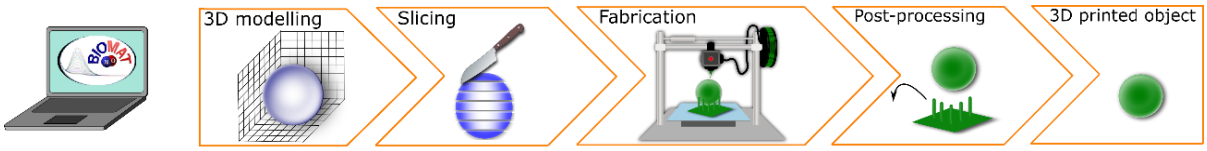

Figure 5. Schematic representation of a 3D printing process chain.

The fabrication method in the 3D printing depends mainly on the material and the application of the printed model. Among the existent methods, inkjet-, extrusion- and photopolymerization-based 3D printing are the currently applied techniques to obtain hydrogel constructs,[46] as shown by a simplified scheme in **Fig. 6**.

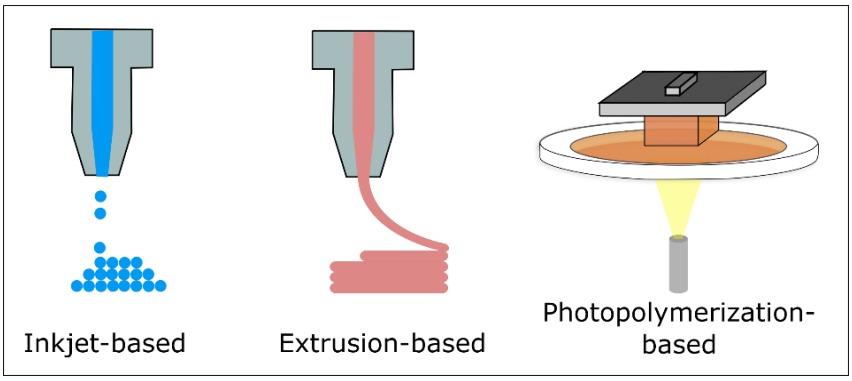

Figure 6. Simplified representation of the available technologies for hydrogel 3D printing.

Inkjet-based 3D printing bears resemblance to ordinary paper printers, considering that drops of a hydrogel precursor are deposited during layer formation.[47] Several works have applied this approach to build cell-laden hydrogels[48,49] by using bioinks containing cells, growing factors and biocompatible supporting polymers. However, the great dependence on rheological parameters is one of the major drawbacks of this technique.[47] Extrusion-based printing combines hydrogel deposition through a nozzle with different solidifying methods, which can be an increase in viscosity after deposition (*i.e.* shear-thinning effect)[50,51] or a cryogenic cooling of the hydrogel,[52] just to name a few. The compatibility with multimaterial printing, along with the diversity in crosslinking methods, are major advantages of this technique. Still, rheology plays an important role in resolution, which is lower than that showed by other hydrogel printing methods.

Photopolymerization-based printing provides the best dimensional control compared to the previously described techniques. It relies on selective irradiation and curing of photopolymerizable mixtures (resins), with help of appropriate photoinitiators, which are capable to generate free-radicals when exposed to light and initiate a polymerization reaction.[53] Particularly, in Digital Light Processing (DLP) printing, bidimensional (2D) light patterns are created by a light source associated with an array of micromirrors (Digital Micromirror Device – DMD). The individual tilting of these mirrors focuses the light on selected spots in the resin and generates a printing layer all at once. In general, the light source is placed under a resin tray containing a transparent window and the 3D model is built layer-by-layer onto a liftable platform.

Some examples of DLP printing applications involving PAA hydrogels were reported by Sujan & Cohn (2017),[54] regarding the copolymerization of AA and methacrylate-functionalized F127 to obtain pH- and thermoresponsive hydrogels and by Jin and coworkers (2016),[55] who applied DLP to build miniaturized PAA-based pH-sensors, with a sub-micron vertical resolution of 0.2 µm.

DLP printing is faster than other photopolymerization-based methods, since its printing speed depends essentially on the number of layers (model height). Commercial printers can reach xy-plane resolutions as low as 25 µm.[56] Vertical plane resolution relates to light penetration and can be tuned by photoblocking agents, reaching values of a few microns.[55,56] Still, the DLP technique has limitations regarding printing of cell-laden constructs, due to cellular damage caused by resin components and light exposure.

Additionally, photoinitiators and photoblockers are generally poorly soluble in water and require using of unfriendly organic solvents.[57] In this regard, the DLP 3D printing of PAA hydrogels in the presence of F127, such as proposed in this work, is an interesting strategy to integrate printing additives through a more biological friendly approach, owing to the F127 surface-activity, which helps to solubilize high amounts of the printing additives in water.

Nitric Oxide (NO)

Nitric oxide (NO) releasing medical devices have been increasingly proposed, given the central role of NO in processes such as vascular homeostasis, angiogenesis and platelet adhesion.[58] NO is a diatomic molecule produced endogenously from L-arginine and has a radical character. Despite of its reactivity against paramagnetic species like O_2, and short half-life in solution,[59] NO is capable to diffuse across cell membranes and interact with biological targets as a signaling agent. Studies in murine models indicate that NO helps wound healing by stimulating re-epitalization and collagen synthesis.[60] Besides, it is suggested that NO has a protective role in cartilage tissues.[61]

The biological effects of NO are highly dependent on its concentration in the cell environment. *In vitro* studies have shown that exposing cells to pico- to nanomolar NO concentrations resulted in cell survival and proliferation[62] and motivated the development of new drugs and platforms for a controlled release of NO. Instead of releasing the gaseous and unstable NO itself, current research focus on the application of compounds able to release NO *in situ*, named NO donors.[63]

The S-nitrosothiols are an important class of NO donors and have a NO group bound to a sulfur atom (-S-N=O), which can be released under influence of light, temperature, transition metals, free thiols and several enzymes.[64] S-nitrosothiols present advantages against other NO donors, since some of them are endogenously found and are intrinsically non-toxic. Besides, biological tests indicate their use as antiplaquetary agents, without risk from tolerance induction under prolonged use.[63] The S-nitrosoglutathione (GSNO) is a low-molar mass endogenous S-nitrosothiol, formed by a tripeptide containing a -SNO moiety attached to a primary carbon (**Fig. 7**).

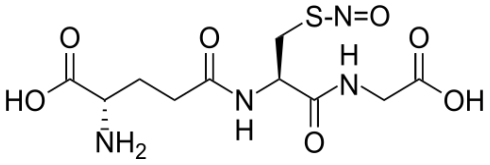

Figure 7. Molecular structure of S-nitrosoglutathione (GSNO).

The efficacy of GSNO on the inhibition of platelet activity has been tested in patients with cardiovascular diseases, without causing hypotension.[65] Besides, GSNO has been linked to angiogenesis *in vitro* on human cells[66] and animal models.[67] The combination of such effects could be explored to obtain less thrombogenic implants and medical devices, with a reduced probability of rejection in the acute inflammatory phase after surgery.

Hydrogels have emerged as candidates for the exogenous NO release since biocompatible hydrophilic polymers can be used to release drugs locally. In these materials, NO donors can be chemically attached to the polymer chain[68] or can be dispersed into hydrogels. Topical formulations comprising GSNO-containing F127 hydrogels were successfully applied in topical vasodilation and wound healing.[69,70] Recently, our research group produced supramolecular hydrogels, comprised of PAA in the presence of a F127 gel. These hydrogels were thermally crosslinked in glass molds, for 24h. The resulting materials were charged with GSNO by swelling in drug aqueous solutions and applied onto wounds in rats, showing improved healing than control hydrogels.[30] This work follows this line of thought and proposes to print these hydrogels in the presence of CNC and introduce GSNO in the sequence.

Despite the therapeutic potential of GSNO, there is no widespread clinical application of this compound up to date, due to its low thermal stability, particularly in the presence of light and water. Consequently, the development of GSNO-charged hydrogels as platforms for NO release is a promising strategy to increase GSNO life span. Up to date, no references were found in the literature regarding semi-IPN PAA-based hydrogels containing F127 and CNC simultaneously, charged with GSNO for the NO release. This choice of components, allied to the 3D fabrication, which is still little explored with NO-releasing materials, may expand the range of GSNO biomedical applications.

General objectives

This work aims at the 3D printing of semi-IPN hydrogels based on PAA, F127 and CNCs (PAA/F127/CNC) using a commercial DLP device, together with a novel method to produce the printable mixtures, in the absence of organic solvents. Moreover, this work seeks to investigate the influence of CNC content on the hydrogel mechanical properties and the kinetics of NO release.

Explanatory note

This master dissertation is organized in three chapters. **Chapter 1** focuses on the development of semi-IPN PAA/F127 and PAA/F127/CNC photopolymerizable hydrogel formulations. The influence of variables such as the reaction time, monomer and crosslinker concentration on hydrogel physico-chemical properties was studied. Particularly, mechanical properties were evaluated with the help of Design of Experiment (DOE) tools. **Chapter 2** presents, in form of a manuscript, the 3D printing of PAA/F127/CNC hydrogels via DLP technique and the study of CNC influence on morphology, compression properties, swelling and kinetics of NO release. Lastly, **Chapter 3** shows preliminary results of the indirect testing of PAA/F127/CNC cytotoxicity against Vero cells, comparing samples washed with ethanol or PBS solution.

Chapter 1. Development of PAA/F127 and PAA/F127/CNC hydrogels

Abstract

This chapter focuses on the development of semi-IPN PAA/F127 and PAA/F127/CNC hydrogel formulations. Herein, the reaction time, monomer (AA) and crosslinker (MBA) concentrations, as well as the CNC content were treated as experimental variables. Lastly, design of experiments (DOE) was employed to analyze the effect of these variables in hydrogel mechanical properties. This strategy was important for further 3D printing of PAA/F127/CNC hydrogels and indicated that the overall hydrogel composition, rather than the reaction time, played a central role in defining hydrogel physical properties.

Experimental procedure

Materials

Pluronic® F127 (PEO_{99}-PPO_{65}-PEO_{99}) of 12,600 g mol^{-1} nominal molar mass, acrylic acid (AA, 99%, containing 200 ppm 4-methoxyphenol - MEHQ inhibitor), photoinitiator Irgacure® 819 – phenylbis(2,4,6-trimethylbenozoylphosphine) oxide (97%), sodium phosphate monobasic monohydrate ($NaH_2PO_4.H_2O$, ≥98%) and sodium phosphate dibasic anhydrous (Na_2HPO_4, ≥98%) were acquired from Sigma Aldrich (St. Louis – MI, USA). N,N'-methylenebisacrylamide – MBA (96%) was obtained from Acros Organics (Geel, BE). Reagents were used without previous purification steps. Cellulose nanocrystals – CNC (nominal width: 5-20 nm; length: 150-200 nm) were acquired as an aqueous gel (11.5-12.5 wt% CNCs) from the University of Maine (Orono – ME, USA) and further dialyzed in deionized water for 5 days to remove salts and preservatives, resulting in a 9.21 wt% aqueous suspension. All the solutions were prepared with deionized water from a Direct-Q 3 UV system (Merck Millipore – Burlington, MA, USA).

Synthesis of semi-IPN PAA/F127 and PAA/F127/CNC hydrogels

Preparation of F127 stock solution

A 35% wt% F127 stock solution was prepared according to the method described by Schmolka (1972).[26] Briefly, 65 g of cold water were weighted in a bottle-necked flask. In the sequence, 35 g of F127 were added under stirring and the flask was stored at 4°C until complete polymer solubilization.

Hydrogel photopolymerization

Semi-IPN hydrogels based on PAA and F127 (PAA/F127) and their counterparts containing CNCs (PAA/F127/CNC) were produced via free-radical photopolymerization. As an example, 25 g of the PAA/F127 photopolymerizable mixtures were prepared as described in **Fig. 8**: known amounts of crosslinker (MBA) and photoinitiator (Irgacure 819 - 0.00418 g, 0.017 wt%) were weighted (1) and mixed with the monomer (AA) (2). Subsequently, *ca.* 14 g of a previously prepared 35 wt% F127 solution were added and homogenized under magnetic stirring in an ice bath (3), resulting in a final concentration of 20 wt% F127, in order to obtain F127 micelles in the resin bulk. Addition of known amounts of a previously dialyzed CNC suspension (9.2 wt%) was required to prepare PAA/F127/CNC formulations (4). CNCs were vigorously mixed with the above described monomer-F127 cold solution until a homogeneous

whitish suspension was observed. Finally, the mixture weight was adjusted by adding water (5) and the content was kept protected from light and stored at 4°C for at least 16h to solubilize the F127 and reduce foaming.

Prior to the hydrogel preparation, the mixtures were degassed in ultrasonic bath for 10 min and 10 g of them were transferred to PTFE molds (Ø = 65mm), placed on a leveled heating plate set at 30 °C (6). The molds were kept for 15 min under a low N_2 flux via a 3-necked glass cover (7).

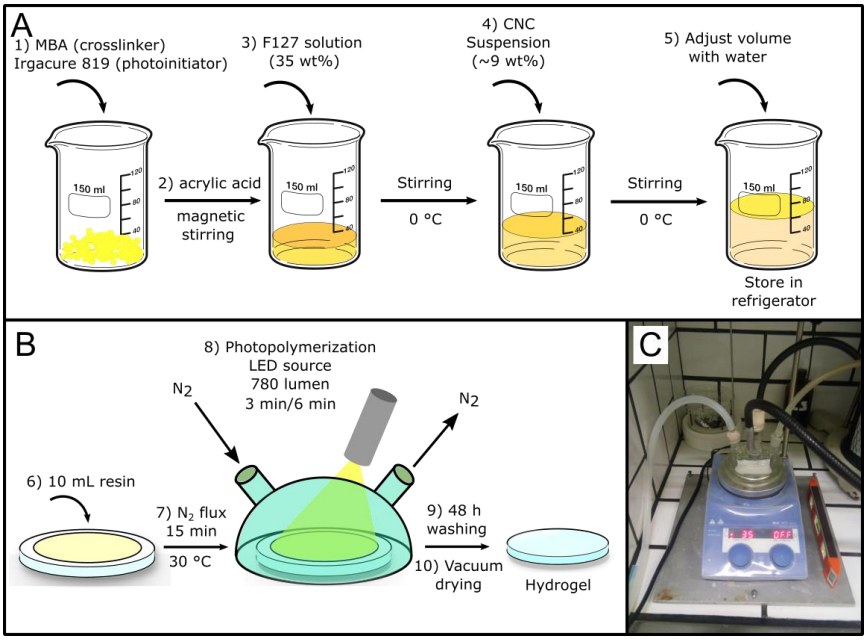

Figure 8. Experimental scheme of the photopolymerizable mixtures preparation: (A), the photopolymerization process (B) and the setup used to obtain PAA/F127 and PAA/F127/CNC hydrogels (C).

After the N_2 purging, The molds were irradiated with an 8W (780 lumen) double-headed LED source (Cole-Parmer, Vermon Hills – IL, US) (8). After light exposure, hydrogels were post-cured with a mercury lamp for 15 min. Samples were then immersed in water for 48 h to remove residues (9) and vacuum dried until constant weight and stored in a desiccator (10).

Hydrogel formulations

Regarding the composition, PAA/F127 hydrogels were developed considering two levels of the monomer (AA) concentration, crosslinker (MBA) concentration and irradiation time,

comprising 8 different formulations. PAA/F127/CNC hydrogels were prepared after preliminary PAA/F127 characterization, which determined beforehand the polymerization time and the AA concentration. In this case, the MBA concentration and CNC concentration were treated as variables, describing 4 different formulations. A summary of the component concentrations for each hydrogel formulation, relative to the total resin feed, as well as photopolymerization time are presented in **Table 1**.

Table 1. Hydrogel component concentrations and polymerization time.

Hydrogel	AA (wt%)	F127 (wt%)	MBA (wt%)	CNC (wt%)	Irgacure (wt%)	AA:MBA ratio	Time (min)
PAA/F127 (AB30/T6)	28.8	20	2.1	0	0.02	30	6
PAA/F127 (AB30/T3)	28.8	20	2.1	0	0.02	30	3
PAA/F127 (AB25/T6)	28.8	20	2.6	0	0.02	25	6
PAA/F127 (AB25/T3)	28.8	20	2.6	0	0.02	25	3
PAA/F127 (AB15/T6)	14.4	20	2.1	0	0.02	15	6
PAA/F127 (AB15/T3)	14.4	20	2.1	0	0.02	15	3
PAA/F127 (AB12/T6)	14.4	20	2.6	0	0.02	12	6
PAA/F127 (AB12/T3)	14.4	20	2.6	0	0.02	12	3
PAA/F127/CNC1.5 (AB30)	28.8	20	2.1	1.5	0.02	30	6
PAA/F127/CNC1 (AB30)	28.8	20	2.1	1	0.02	30	6
PAA/F127/CNC1.5 (AB25)	28.8	20	2.6	1.5	0.02	25	6
PAA/F127/CNC1 (AB25)	28.8	20	2.6	1	0.02	25	6

The hydrogels described in **Table 1** were randomly synthesized and produced in the presence of *ca.* 50 wt% water and 20 wt% F127. PAA/F127 hydrogels were named after the monomer to crosslinker (AA:MBA) molar ratio and the polymerization time. As an example, the PAA/F127 (AB25/T6) sample was produced in the presence of 25:1 AA:MBA molar ratio and 6 min irradiation time. For PAA/F127/CNC hydrogels, time was fixed at 6 min and samples were named after the AA:MBA molar ratio as well as the CNC concentration in the formulation.

Material characterization

Hydrogel swelling

Hydrogel discs were cut by using a surgical punch (Ø=6 mm) and immersed in 2 mL of a 10 mM phosphate buffered saline solution (PBS, pH 7.4) at 25°C. Hydrogels were

removed from solution in defined intervals, and then the surfaces were wiped with filter paper for weighting. Swelling degree was determined according to the **Eq. 1**.

$$Swelling\ ratio\ (g/g) = \frac{m_S - m_0}{m_0} \textbf{ (Equation 1)}$$

where m_S corresponds to the swollen weight and m_0 to the weight of a previously dried hydrogel sample, respectively.

Scanning Electron Microscopy (SEM)

Scanning electron micrographs of dried hydrogel samples were obtained after cryogenic fracture for morphology analysis in a JEOL 6360-LV microscope (JEOL Instruments, Akishima, Tokyo – JP) using a 10 kV acceleration voltage. Samples were mounted onto brass stubs and coated with iridium in a MED 020 sputtering device (BAL-TEC AG, Balzers – LIE) for 180 s and 15.5 mA current.

Infrared Vibrational Spectroscopy (FTIR)

FTIR spectra of dried hydrogel samples and their respective components were acquired in a 630 FTIR spectrometer (Agilent Cary, Santa Clara, CA – US), in the range 4000 – 400 cm^{-1} and ATR mode, by depositing the samples directly onto the ZnSe crystal.

Compression tests – Thermomechanical Analysis (TMA)

The compressive response of the PAA/F127 and PAA/F127/CNC dried hydrogel samples was analyzed in a thermomechanical analyzer (TMA) TA2940 (TA Instruments, New Castle – DE, US). Discs of the samples were cut with surgical punch (Ø = 6 mm; width = ca. 2 mm) and subjected to a single loading-unloading cycle, to a 1 N maximum force, at a constant 0.05 N min^{-1} compression rate and 25 °C temperature. Samples were analyzed in single measurements.

Tensile tests

Tensile properties of the PAA/F127 and PAA/F127/CNC hydrogels were analyzed in a universal test machine EMIC 23-20 (Instron do Brasil, São José dos Pinhais – PR, BR) at room temperature and at 50% relative air humidity, by using dumbbell-shaped specimens cut

from hydrogel samples, according to the ASTM D1708 standard (gauge length: 22 mm; diameter: 5 mm; width: ca. 2 mm). Unless specified, measurements were carried out in duplicate samples.

Design of Experiments (DOE)

The parameters used in the production of PAA/F127 hydrogels were screened to define a formulation to be employed in the 3D printing process. A complete 2^3 factorial design was proposed, according to Barros et al.,[71] to evaluate the effects of experimental variables in the tensile Young's moduli of the photopolymerized PAA/F127 hydrogels. Herein, each factor varied between two levels: AA concentration (low - 2 mol L^{-1}, high - 4 mol L^{-1}), MBA concentration (low - 0.13 mol L^{-1}, high - 0.16 mol L^{-1}) and LED irradiation time (low - 3 min, high - 6 min).

Briefly, this methodology stems from a linear model, which describes a response surface based on variations in independent factors and their interactions, as given by **Eq. 2**

$$y = \beta_0 + \sum_i^k \beta_i Xx_i + \sum_{ij}^k \beta_i Xx_i Xx_j + \sum_{ijk}^k \beta_i Xx_i Xx_j Xx_k + \varepsilon \text{ (**Equation 2**)}$$

In the above described linear model, y represents the points which enclose a response surface. In this work, the response relates to the Young's modulus (YM) values obtained from tensile tests of PAA/F127 hydrogels. The β_i coefficients represent the intercept (β_0) and individual factor contributions to the model (*i.e.* β_1: AA concentration; β_2: MBA concentration and β_3: polymerization time), whereas β_{ij} (β_{12}, β_{13} and β_{23}) and b_{ijk} (β_{123}) refer to interactions between two and three factors, respectively.

After fitting the model to the response values, analysis of variance (ANOVA) was carried out to validate it by using the software Minitab 19 (Minitab Inc., State College – PA, USA). Considering the ANOVA results, the coefficient β_{123} was truncated and used to obtain the standard error for the model coefficients.

Results and Discussion

Hydrogel photopolymerization

PAA/F127 hydrogels were produced via photopolymerization and molded as discs, following the formulations described in **Table 1**. Images of the synthesized hydrogels after lyophilization are shown in **Fig. 9**.

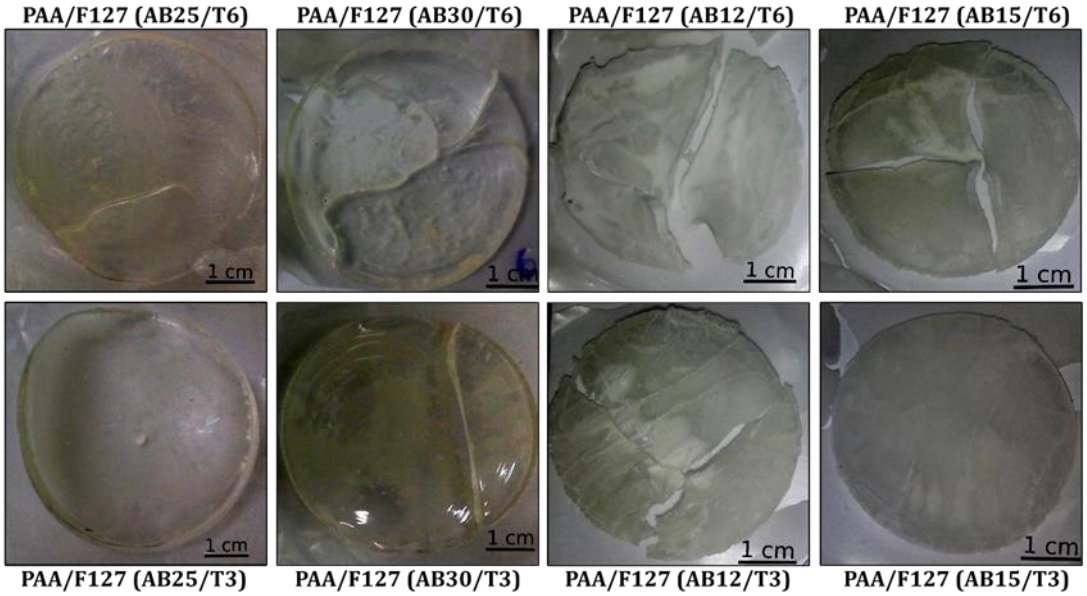

Figure 9. Representative images of dried PAA/F127 hydrogel discs.

According to **Fig. 9**, the overall composition plays an important role in determining the hydrogel properties. The hydrogels prepared in the presence of high monomer concentration (high AA:MBA ratios - AB25 and AB30 samples) were transparent and flexible even after the drying procedure. Samples coded as AB12 and AB15 (small monomer concentration) resulted in brittle pieces with irregular surfaces and an opaque appearance. Hydrogels tended to present cracks due to the freezing process employed for drying. In this sense, in subsequent processes, samples were dried at room temperature, what required extended drying periods.

Alternatively, PAA/F127/CNC hydrogels were prepared after fixing polymerization time (6 min) and the monomer concentration (4 mol L^{-1}). Four different formulations were developed by employing 1 wt% or 1.5 wt% CNCs and 25:1 or 30:1 AA:MBA molar ratio, as shown in **Table 1**. PAA/F127/CNC hydrogel samples are depicted in **Fig. 10**.

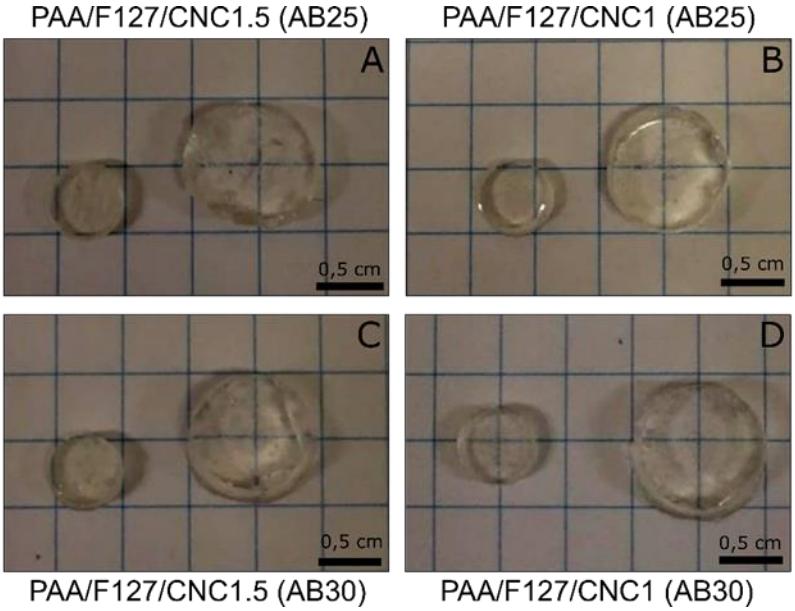

Figure 10. Images of PAA/F127/CNC hydrogels in dry and swollen state. (A) PAA/F127/CNC1.5 (AB25), (B) PAA/F127/CNC1 (AB25), (C) PAA/F127/CNC1.5 (AB30), (D) PAA/F127/CNC1 (AB30).

PAA/F127/CNC hydrogels were largely similar to hydrogels produced in the absence of CNCs (PAA/F127) under the same experimental conditions. Samples exhibited flexibility during handling and preserved transparency when dried, due to the low CNC content employed.

Hydrogel Swelling

Water swelling is a key property to define applications of hydrogels, as it is intimately related to drug release profiles and to dimensional changes. The swelling profiles of PAA/F127 hydrogels were obtained during 24 h in 0.01 M PBS buffer (pH 7.4) at 25°C, as shown in **Fig. 11**.

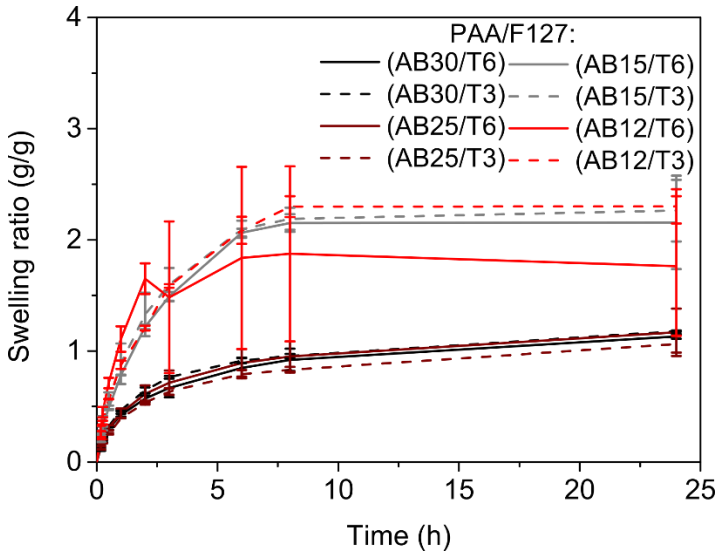

Figure 11. Swelling profiles of PAA/F127 hydrogels in 0.01 M PBS (pH 7.4) at 25 °C for 24 h.

According to **Fig. 11**, PAA/F127 hydrogels can be arranged in two groups: the first is represented by samples produced with high monomer concentration, *i.e.* 25:1 (AB25) and 30:1 (AB30) AA:MBA molar ratios. These hydrogels exhibited lower swelling rates and equilibrium swelling ratio than samples of the second group, which encompasses hydrogels produced with 12:1 (AB12) and 15:1 (AB15) AA:MBA ratios. The hydrogels produced with a small monomer concentration presented not only faster swelling and higher equilibrium swelling than their counterparts but resulted in more fragile samples when handled during the experiment. This result is reasonable, since properties intimately related to the swelling behavior, such as the crosslinking density and the gel fraction are affected by the monomer and crosslinker concentrations.[2]

It is important to mention that a characteristic of semi-IPN hydrogels is the possibility of the non-crosslinked polymers to be extracted. In the PAA/F127 hydrogels, the extraction of F127 was noted due to foam formation during the swelling measurements. Additionally, in the AB12 and AB15-type hydrogels, F127 leakage was intense due to lower crosslinking density and to hydrogels breaking during handling, resulting in high mean deviations. Considering the reproducibility of the swelling profiles and the structural stability of the photopolymerized PAA/F127 hydrogels, PAA/F127/CNC hydrogels were produced using high monomer concentration and monomer to crosslinker ratios (AA:BIS = 25:1 or 30:1).

The swelling behavior of the PAA/F127/CNC samples was analyzed similarly to the PAA/F127 hydrogels. Hydrogels were immersed in PBS buffer until swelling equilibrium was achieved (**Fig. 12**).

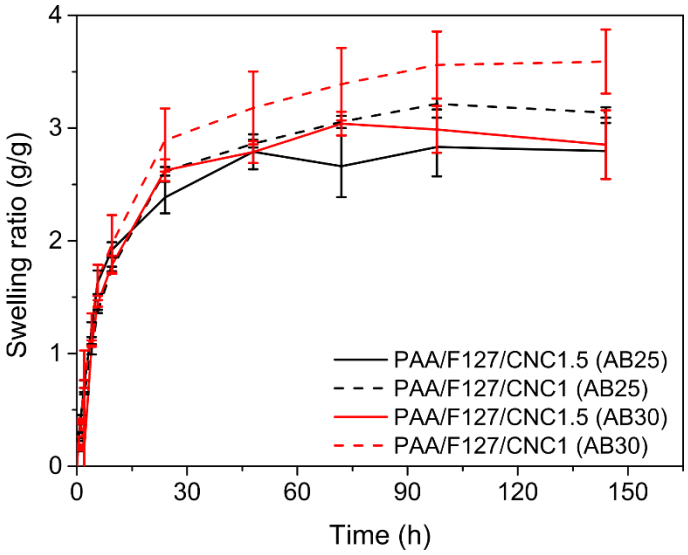

Figure 12. Swelling profiles of PAA/F127/CNC hydrogels in 0.01 M PBS buffer (pH 7.4) at 25 °C.

The incorporation of CNCs in hydrogel formulations increased swelling in approximately three times, compared to the samples shown in **Fig. 11**, which were produced under the same AA:MBA ratios (25:1 and 30:1). Moreover, swelling equilibrium was reached after four days. As reported by Lim et al.,[72] the presence of small CNC contents (up to 5 wt% relative to monomer mass) increases the number of available hydrophilic groups and consequently leads to increases in PAA hydrogel swelling ratio. Hydrogel formulations containing 1 wt% CNCs resulted in higher swelling than that with 1.5 wt% CNCs, probably due to a barrier effect to water, caused by CNCs. Particularly, PAA/F127/CNC1 (AB30) exhibited the highest swelling among the analyzed samples, a feature that may be related to a less dense hydrogel matrix, given the lower crosslinker and CNC concentrations.

Infrared Vibrational Spectroscopy (FTIR)

Transmittance infrared spectra in ATR mode were acquired to assess hydrogel crosslinking and to compare hydrogels produced from different formulations: PAA-only,

PAA/F127 and PAA/F127/CNC1 hydrogels (**Fig. 13**). Hydrogels were synthesized according to the same procedure and AA:MBA ratio was fixed at 25:1.

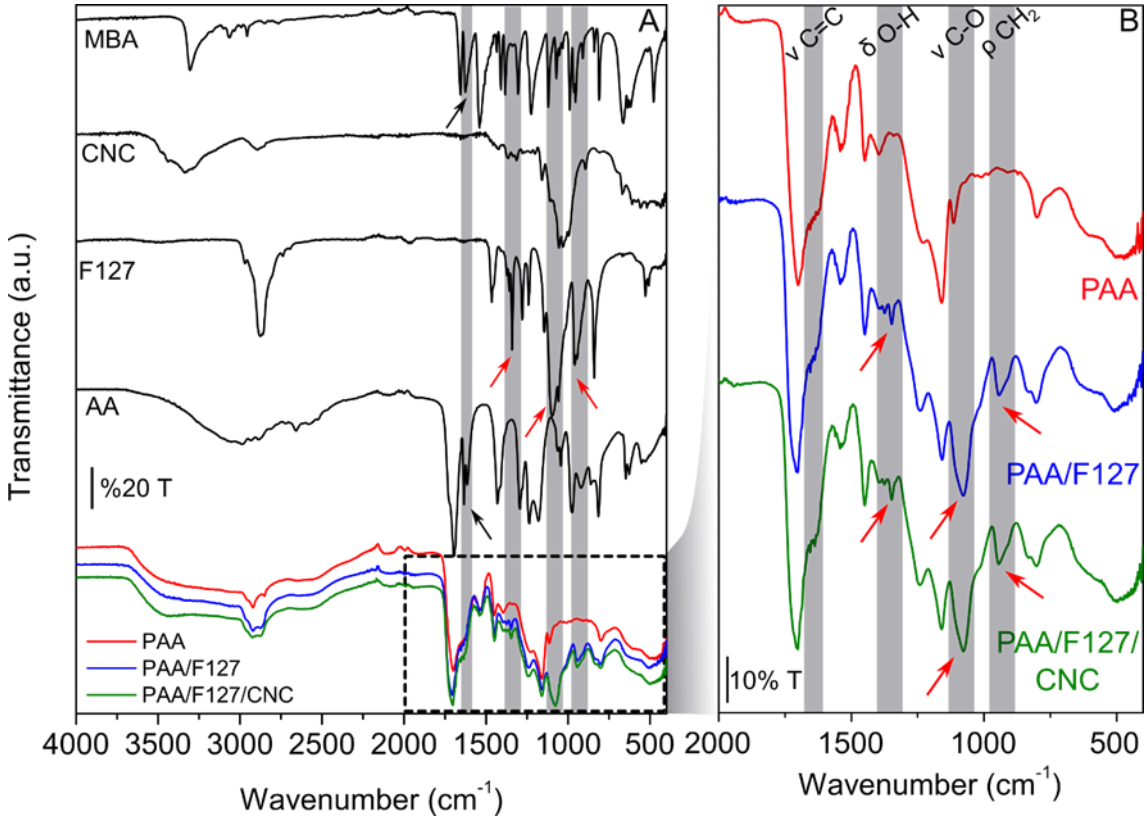

Figure 13. FTIR-ATR spectra of PAA/F127/CNC (A) hydrogel components acquired between 4000 cm^{-1} and 400 cm^{-1}. (B) The onset graph is a magnification in the range from 2000 cm^{-1} to 400 cm^{-1} of PAA (AB25) (red), PAA/F127 (AB25) (blue) and PAA/F127/CNC1 (AB25) (green) hydrogel spectra. The arrows highlight major differences between hydrogels and their components.

In the **Fig. 13A**, the main assignments in the AA spectrum were a large O-H stretching band between 3650 cm^{-1} and 2750 cm^{-1}, a strong C=O stretching band centered at 1696 cm^{-1}, along with a C=C stretching at 1632 cm^{-1}.[73,74] The MBA spectrum shows bands at 3305 cm^{-1} (N-H stretching), 3105 cm^{-1} (CH_2 stretching), 1655 cm^{-1} (C=O stretching - amide I band), 1627 cm^{-1} (C=C stretching), 1539 cm^{-1} (N-H bending – amide II) and 1304 cm^{-1} (C-N bending – amide III).[75] The F127 presents in its FTIR spectrum a C-H stretching vibration at 2884 cm^{-1}, strong bands at 1342 cm^{-1}, 1040 cm^{-1} and 960 cm^{-1}, assigned to in-plane bending of O-H bonds, C-O stretching and CH_2 rocking vibration, respectively.[76,77] Lastly, the FTIR

spectrum of lyophilized CNCs shows a large O-H stretching band, centered at 3300 cm^{-1} and C-H stretching band at 2894 cm^{-1}. The strong vibration band around 1060 cm^{-1} was assigned to C-O stretching in pyranose units.[78]

The comparison between a set of hydrogel spectra with those obtained from the main components, as depicted in the onset graph (**Fig. 13B**), reveals that characteristic monomer (AA and MBA) vinyl stretching bands (black arrows in **Fig. 13A**) were absent in all hydrogel samples, suggesting that the photopolymerization process resulted in high conversion of these reactive groups. The appearance of δ O-H (1348 cm^{-1}), ν C-O (1077 cm^{-1}) and ρ CH_2 (943 cm^{-1}) bands in PAA/F127 and PAA/F127/CNC spectra, as highlighted by the red arrows in **Fig. 13B**, stems from F127, which are absent in PAA hydrogels. Additionally, these δ O-H and ν C-O bands in hydrogels were shifted towards higher wavenumbers compared to pure F127, although ρ CH_2 band was shifted to lower wavenumbers. The carbonyl bands, derived mainly from AA, were also shifted in the hydrogel spectra. In PAA hydrogels, C=O band was centered at 1700 cm^{-1}. In PAA/F127 and PAA/F127/CNC hydrogel spectra, the same band was found at 1705 cm^{-1}. The observed shifts in absorption maxima suggest that intermolecular interactions between F127 and PAA carbonyl groups may be present in hydrogel structure, and consequently forming a semi-IPN network.[79] Lastly, CNC contributions to the PAA/F127/CNC spectrum were undistinguishable from other bands, given the low CNC content.

Scanning Electron Microscopy (SEM)

Scanning electron micrographs of cryogenically fractured PAA/F127 hydrogels, were obtained for morphological analysis and are shown in **Fig. 14**.

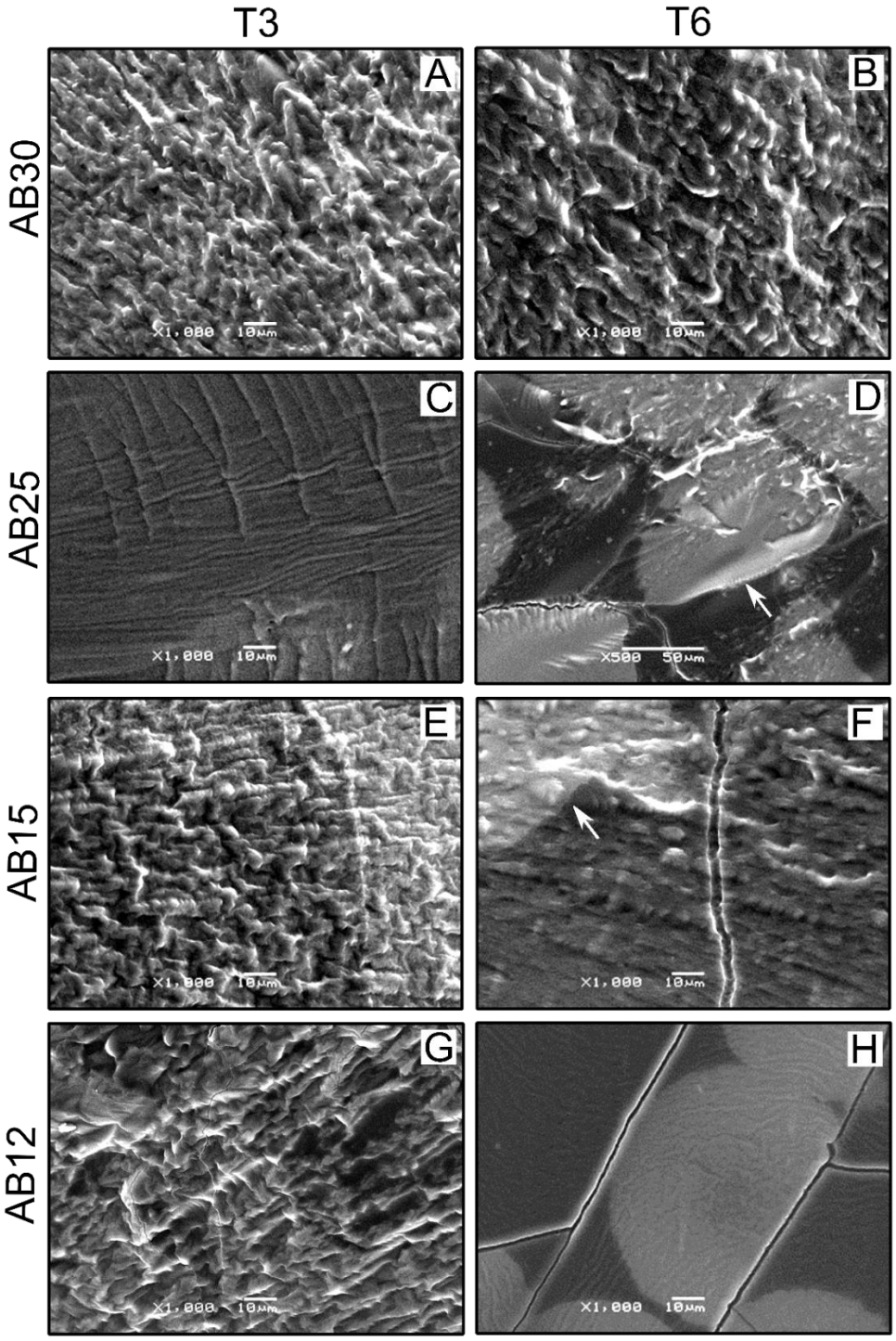

Figure 14. Representative cross-sectional SEM micrographs of PAA/F127 hydrogels. (A) AB30/T3; (B) AB30/T6; (C) AB25/T3; (D) AB25/T6; (E) AB15/T3; (F) AB15/T6; (G) AB12/T3; (H) AB12/T6. The arrows highlight regions of clear tonalities

The analyzed PAA/F127 hydrogels presented dense morphologies, without pores. However, cracks in hydrogel cross-sections were observed in AB25/T3 **(Fig. 14F)**, AB15/T6

(Fig. 14G), AB12/T3 **(Fig. 14G)** and in AB12/T6 samples **(Fig. 14H)**. The presence of cracks after hydrogel drying occurred due to brittleness induced by the simultaneous decrease in monomer and increase in crosslinker concentrations. Moreover, in samples AB25/T3 (**Fig. 14C**), AB25/T6 (**Fig. 14D**), AB15/T6 (**Fig. 14F**) and AB12/T6 (**Fig. 14H**), the white arrows indicate regions with different tonalities compared to hydrogel bulk, which could be related to changes in local composition. In summary, PAA/F127 (AB30) hydrogels (**Fig. 14A, Fig. 14E**) resulted in the most uniform samples and were the least prone to cracks.

The PAA/F127/CNC hydrogels were also investigated, and cross-sectional images are shown in **Fig. 15**.

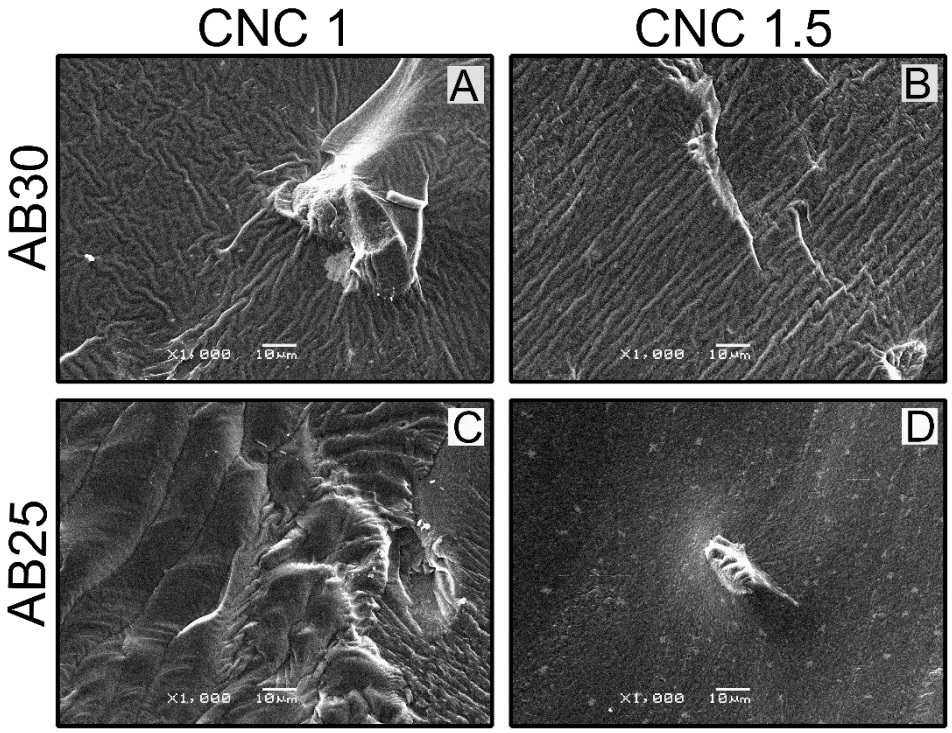

Figure 15. Representative cross-sectional SEM micrographs of PAA/F127/CNC hydrogels: (A) PAA/F127/CNC1 (AB30), (B) PAA/F127/CNC1.5 (AB30), (C) PAA/F127/CNC1 (AB25), (D) PAA/F127/CNC1.5 (AB25).

The synthesis of hydrogels in the presence of CNCs was carried out using 25:1 and 30:1 AA:MBA molar ratios, since in these conditions PAA/F127 hydrogels were the most uniform, compared to hydrogels containing lower AA:MBA ratios. The micrographs shown in **Fig. 15** reveal that PAA/F127/CNC hydrogels have smooth fractures and dense

morphologies, suggesting that CNC incorporation does not affect substantially the hydrogel morphology, compared to the corresponding PAA/F127 samples. A remarkable feature is presented by the PAA/F127/CNC1.5 (AB25) hydrogel (**Fig. 15D**), due to the appearance of dots on the fracture surface, which suggests the presence of CNC aggregates. These aggregates could be formed by incomplete homogenization during the photopolymerizable mixture preparation.

Mechanical properties

The investigation of mechanical behavior is of major importance for biomedical applications of hydrogels, since the materials must be designed to mimic the properties of a host tissue. With this aim, the compressive properties of dried PAA/F127 and PAA/F127/CNC hydrogels were evaluated by unconfined compression tests at 25 °C. The samples were subjected to a single loading/unloading cycle at a constant compression rate. Stress *versus* strain graphs were plotted as shown in **Fig. 16**.

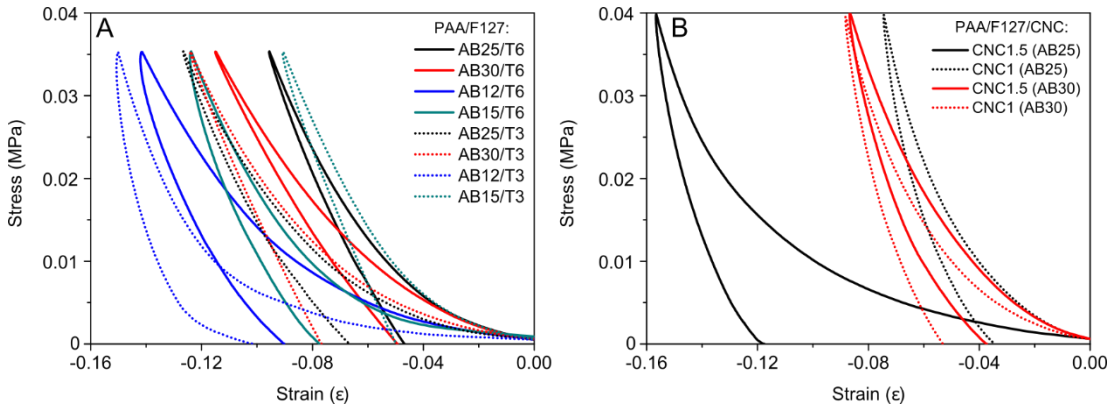

Figure 16. Compressive stress *versus* strain curves for (A) PAA/F127 hydrogels and (B) PAA/F127/CNC hydrogels.

Compressive experiments were performed to a maximum force of 1 N, which resulted in low deformations (max. 16%). All hydrogels exhibited a viscoelastic behavior under compression and did not fully recover their original dimensions after loading removal. The stress *versus* strain curves displayed in **Fig. 16** show hysteresis, which indicates a permanent deformation of the hydrogels and relates to the energy dissipation during the compression cycle.[80] Furthermore, to investigate the influence of polymerization time and overall composition in the compressive properties, compressive moduli were calculated as the initial

slope of PAA/F127 (**Fig. 16A**) and PAA/F127/CNC (**Fig. 16B**) hydrogel loading curves from each measurement. The results are listed in **Table 2**.

Table 2. Compressive moduli of PAA/F127 and PAA/F127/CNC hydrogels.

Hydrogel	Compressive modulus (MPa)
PAA/F127 (AB30/T6)	0.052
PAA/F127 (AB30/T3)	0.040
PAA/F127 (AB25/T6)	0.067
PAA/F127 (AB25/T3)	0.031
PAA/F127 (AB15/T6)	0.028
PAA/F127 (AB15/T3)	0.055
PAA/F127 (AB12/T6)	0.034
PAA/F127 (AB12/T3)	0.016
PAA/F127/CNC1.5 (AB30)	0.089
PAA/F127/CNC1 (AB30)	0.058
PAA/F127/CNC1.5 (AB25)	0.044
PAA/F127/CNC1 (AB25)	0.086

PAA/F127 hydrogels produced from low monomer concentrations (AB12 and AB15 samples) exhibited higher deformation and a more viscous behavior than samples AB25 or AB30. The predominant viscous behavior and the permanent deformation presented by AB12 and AB15 are undesirable considering that this work intends to develop candidate materials for tissue implants.

Moreover, hydrogels exposed to a longer photopolymerization time (T6 samples), tended to display an increase in compressive strength, since they were less deformable and resulted in higher moduli than T3 samples. These results suggest that not only the monomer concentration, but also the irradiation time was a relevant parameter to determine hydrogel compressive properties. Possibly, the network density was affected mainly by composition and in less extent by reaction time since low polymerization conversion can lead to inhomogeneities.

PAA/F127/CNC hydrogels (**Fig. 16B**) exhibited a viscoelastic compressive behavior, comparable to corresponding PAA/F127 samples (AB25 and AB30). However, according to **Table 2**, CNC introduction apparently increased hydrogel compressive moduli, with exception of PAA/F127/CNC1.5 (AB25) sample. Additionally, trends in moduli related to CNC proportion could not be observed, possibly due to the small differences in CNC concentration used.

Tensile properties of dried PAA/F127 and PAA/F127/CNC hydrogel samples were assessed via strain tests. Stress-strain curves of the tested hydrogels are shown in **Fig. 17**.

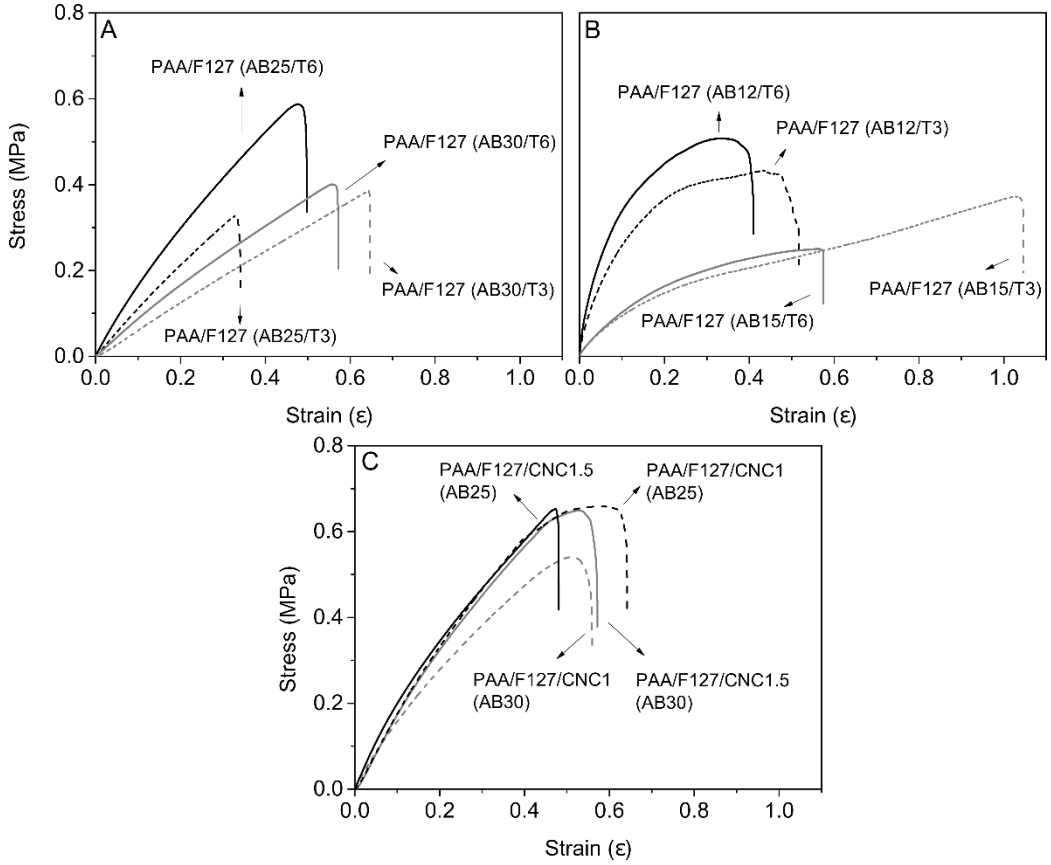

Figure 17. Typical stress-strain curves of PAA/F127 and PAA/F127/CNC hydrogels. (A) PAA/F127 (AB25) and PAA/F127 (AB30); (B) PAA/F127 (AB12) and PAA/F127 (AB15); (C) PAA/F127/CNC hydrogels. In (**A**) and (**B**), solid curves represent hydrogels polymerized during 6 min and dashed curves relate to a 3 min photopolymerization time.

Tensile tests of PAA/F127 (AB25) (**Fig. 17A**, black) and PAA/F127 (AB30) (**Fig. 17A**, grey) resulted in linear behavior, followed by rupture, indicating that these samples were predominantly elastic when subjected to stress. On the other hand, PAA/F127 (AB12) (**Fig. 17B**, black) and PAA/F127 (AB15) (**Fig. 17B**, grey) hydrogels presented a distinct viscous behavior. These samples were also rigid, as noticed by higher slopes on the initial linear regions, when compared with samples prepared with higher monomer concentrations. Moreover, cracks occurred during AB12 and AB15 hydrogel handling and drying, what induced premature breaking under stress and limited the number of analyzed samples to a single measurement per composition.

The strain properties of PAA/F127/CNC hydrogels (**Fig. 17C**) were investigated by using four replicate samples and exhibited similar stress-strain profiles as to the correspondent PAA/F127 hydrogels (AB25 and AB30). However, introduction of CNCs seems to increase resistance to strain, noticed by an apparent increase in the slopes, while keeping the predominant elastic behavior. The curves shown in **Fig. 17** were used to obtain the Young's modulus (YM), ultimate stress and elongation at break of the hydrogels. These data were summarized in **Table 3**, which were averaged only for PAA/F127/CNC hydrogels.

Table 3. Young's Modulus, ultimate stress and elongation at break values, calculated from stress-strain curves of PAA/F127 and PAA/F127/CNC hydrogels.

Hydrogel	Young's modulus (MPa)	Ultimate stress (MPa)	Elongation at break (ε)
PAA/F127 (AB30/T6)	0.92±0.04	0.50±0.01	0.57±0.01
PAA/F127 (AB30/T3)	0.76±0.16	0.51±0.05	0.64±0.01
PAA/F127 (AB25/T6)	1.62±0.17	0.67±0.08	0.56±0.11
PAA/F127 (AB25/T3)	1.06±0.10	0.40±0.04	0.35±0.03
PAA/F127 (AB15/T6)*	1.23	0.32	0.56
PAA/F127 (AB15/T3)*	1.04	0.42	1.03
PAA/F127 (AB12/T6)*	7.10	0.56	0.34
PAA/F127 (AB12/T3)*	4.59	0.55	0.43
PAA/F127/CNC1.5 (AB30)	2.15±0.42	0.68±0.07	0.51±0.14
PAA/F127/CNC1 (AB30)	1.60±0.13	0.55±0.08	0.48±0.05
PAA/F127/CNC1.5 (AB25)	2.24±0.34	0.64±0.11	0.46±0.05
PAA/F127/CNC1 (AB25)	1.87±0.17	0.64±0.11	0.59±0.02

*single measurements

The results show that dried PAA/F127 hydrogels can support ca. 0.5 MPa ultimate stress. Particularly, the AB25/T6 hydrogel, produced under the longest polymerization time and highest monomer and crosslinker concentrations, reached the highest stress among the PAA/F127 samples. The average maximum strain was ca. 55%, which is an intermediary value considering the existence of hydrogels capable to maintain much higher elongations.[81,82] Additionally, YM values of ca. 1 MPa were obtained for PAA/F127 hydrogels, excluding AB12-like samples.

PAA/F127/CNC hydrogels presented higher YM and ultimate stress values than equivalent PAA/F127 hydrogels, keeping the average elongation at break. YM values of PAA/F127/CNC1.5 hydrogels were higher than corresponding values presented by PAA/F127/CNC1 samples. These results suggest that CNCs acted as a reinforcing agent for PAA/F127/CNC hydrogels.

Design of Experiments (DoE)

The trends in YM values related to the composition of PAA/F127 hydrogels were further investigated considering a complete 2^3 factorial design, where the AA and MBA concentration, as well as the time of LED irradiation were the factors used to fit the YM values response, as shown in **Table 4**.

Table 4. Variables of a complete 2^3 factorial design for YM values obtained from tensile tests of PAA/F127 hydrogels.

		- 1	+1		
Factors	**A:** AA concentration (mol L^{-1})	2	4		
	B: MBA concentration (mol L^{-1})	0.13	0.16		
	C: Irradiation time (min)	3	6		
Trial	**Hydrogel**	**A**	**B**	**C**	**YM (MPa)**
1	PAA/F127 (AB30/T6)	+1	-1	+1	0.89
2	PAA/F127 (AB30/T6)	+1	-1	+1	0.95
3	PAA/F127 (AB30/T3)	+1	-1	-1	0.87
4	PAA/F127 (AB30/T3)	+1	-1	-1	0.65
5	PAA/F127 (AB25/T6)	+1	+1	+1	1.74
6	PAA/F127 (AB25/T6)	+1	+1	+1	1.50
7	PAA/F127 (AB25/T3)	+1	+1	-1	1.13
8	PAA/F127 (AB25/T3)	+1	+1	-1	0.99
9	PAA/F127 (AB15/T6)	-1	-1	+1	1.23
10	PAA/F127 (AB15/T3)	-1	-1	-1	1.04
11	PAA/F127 (AB12/T6)	-1	+1	+1	7.10
12	PAA/F127 (AB12/T3)	-1	+1	-1	4.59

The factorial design was carried out with 12 trials, as AB25 and AB30 samples were analyzed in duplicate. Regression analysis was then applied to obtain the equation coefficients and their standard errors, as shown in **Table 5**. The 3-factor interaction effect (AA + MBA + time) was statistically non-significant and used for estimating the standard errors of the effects in the model, since no central point trial was employed. The effects were standardized (*i.e.* divided by the respective standard deviation) and plotted in a Pareto chart, for a better understanding (**Fig. 18**).

Table 5. Regression analysis of the response surface based on Young's moduli of PAA/F127 hydrogels.

Term	Effect	Coefficient	Standard Error	T-value	P-value
Intercept		2.29	0.11	20.3	0
A	-2.40	-1.20	0.11	-10.64	0.0001
B	2.61	1.30	0.11	11.54	0.0001
C	0.86	0.43	0.11	3.79	0.0128
AB	-2.11	-1.05	0.11	-9.33	0.0002
AC	-0.50	-0.25	0.11	-2.19	0.0797
BC	0.52	0.26	0.11	2.44	0.0584

(A) – AA, (B) – MBA, (C) - time

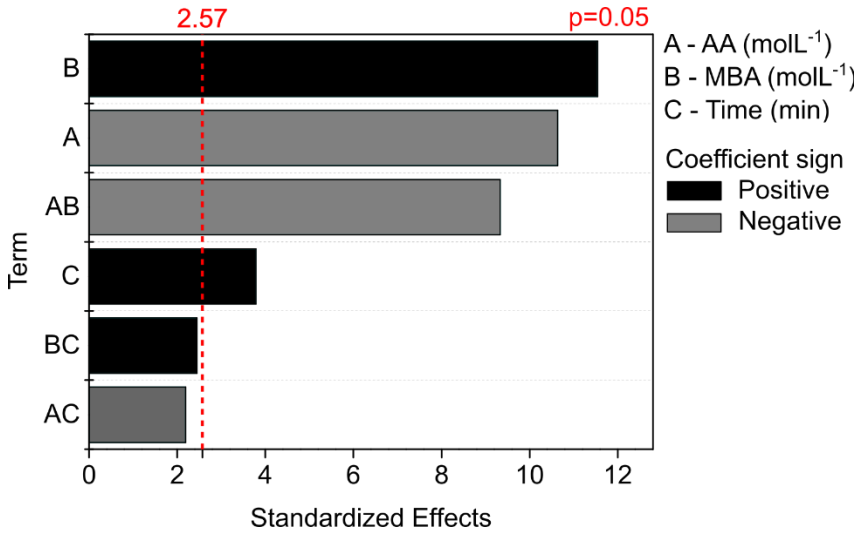

Figure 18. Pareto chart of the standardized effects for YM values of PAA/F127 hydrogels in a complete 2^3 factorial design.

The Pareto chart presented in **Fig. 18** enables the identification of the statistically significant effects, where the vertical line represents the minimum value of significance, considering p=0.05. The results suggest that the effects assigned to the hydrogel composition were statistically significant. Particularly, the increase in MBA concentration (B) caused an increase in the YM values. On the other hand, the AA concentration (A) had the opposite effect. As a result, high AA:MBA ratios (AB) led to low YM values, which were expected and related to flexible PAA/F127 hydrogel samples in the dry state. Consequently, high AA:MBA ratios (*i.e.* AB30-type samples) were recommended for future experiments due to an increased network density, while keeping hydrogel flexibility during handling. The effect

of irradiation time was also significant, however, it played a minor role in defining the YM values in this experiment, with non-significant interactions with the other effects.

Additionally, ANOVA testing was used to evaluate the model applicability, as shown in **Table 6**.

Table 6. Analysis of Variance (ANOVA) test sheet of the linear model proposed in the complete 2^3 factorial design for PAA/F127 hydrogels.

Source	Degrees of Freedom (DF)	Sum of Squares (SS)	Mean Square (MS)	F-value	P-Value
Model	6	40.94	6.82	50.24	0.0003
Linear	3	35.41	11.80	86.91	0.0001
A	1	15.36	15.36	113.11	0.0001
B	1	18.10	18.10	133.26	0.0001
C	1	1.95	1.95	14.35	0.0128
2-factor interactions	3	13.28	4.43	32.60	0.0010
AB	1	11.82	11.82	87.01	0.0002
AC	1	0.65	0.65	4.81	0.0797
BC	1	0.81	0.81	5.97	0.0584
Error	5	0.68	0.14		
Lack of adjustment	1	0.61	0.61	38.04	0.0035
Pure Error	4	0.06	0.02		
Total	11	41.62			
S	0.368511	**R^2(adj)**	96.41%		
R^2	98.37%	**R^2(pred)**	62.36%		

ANOVA testing supports the statistical significance of composition effects (A, B and AB) and time (C). Moreover, R^2 and adjusted R^2 were high, showing that the model fitted well to data. However, the predicted R^2 is low, meaning that the proposed model was not fully optimized for prediction of YM values if theoretical parameters are to be used. Possibly, the model can be improved by increasing the number of experiments and replicates, although it provides help to screen for the factor contributions to YM response. A similar mathematical approach could not be applied to analyze compositional effects in PAA/F127/CNC hydrogels, since data fluctuation produced a poor-quality fitting (results not shown).

The 3D printing of PAA/F127/CNC hydrogels is one of the main objects of this work and is thoroughly explored and explained in Chapter 2. Still, it is worth to mention that preliminary printing tests were performed with PAA/F127 (AB30) formulations, due to the

best performance observed in the screening of mechanical properties through the factorial design, generating objects such as the one displayed in **Fig. 19**.

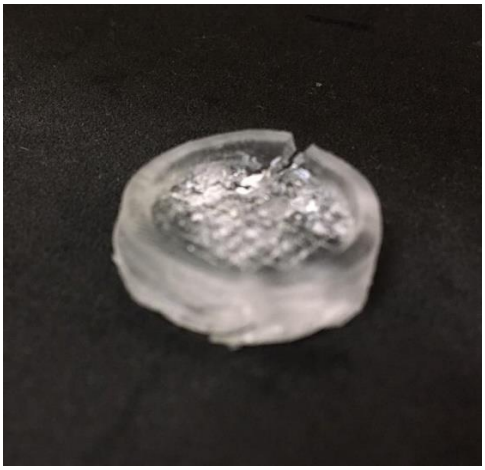

Figure 19. Example of a PAA/F127 (AB30) 3D printed hydrogel net exhibiting a crack

Despite the possibility to obtain 3D printed objects, hydrogel pieces were brittle and of difficult handling, showing cracks during removal from printing head. Moreover, resolution was low due to intense light penetration, which can be improved by addition of photoblockers (dyes). Considering these results, crosslinker concentration had to be 5-fold reduced, resulting in a 150:1 AA to MBA molar ratio, used in further experiments, along with the addition of a dye to improve printing resolution.

Conclusions

PAA/F127 and PAA/F127/CNC hydrogels were synthesized according to an easy and fast photopolymerization process, by using LED irradiation in the visible spectrum range.

The influence of irradiation time and concentration of major hydrogel components (monomer – AA, crosslinker – MBA, and CNCs) in physical properties was studied. As a result, non-porous hydrogels were obtained, according to SEM micrographs, and showed significant dependence on the relative concentrations of AA and MBA in the formulations. A decrease in monomer concentration from ca. 4 mol L^{-1} to 2 mol L^{-1} was followed by a 2-fold decrease in AA:MBA molar ratios (AB25 to AB12 and AB30 to AB15), which impaired hydrogel strain and compressive strength, as well as increased water swelling.

Hydrogel Young's moduli were obtained by linear fitting of stress-strain curves and were employed as responses in a complete 2^3 factorial design for PAA/F127 hydrogels. The

model confirmed a major dependence of mechanical properties on composition, while reaction time acted in a lesser extent to define the YM response.

Additionally, PAA/F127/CNC hydrogels revealed improved mechanical properties when compared to corresponding PAA/F127 hydrogels and an increase in CNC content from 1 wt% to 1.5 wt% resulted in increased YM values

In summary, the results indicate that mechanical properties of semi-IPN PAA/F127 hydrogels can be tuned by CNCs, such as to mimic living tissue features. However, future applications and 3D manufacturing of these materials require further studies, especially regarding the crosslinking density of these networks, which must be improved to avoid material failure and premature cracks in swollen state.

Chapter 2. Nitric oxide-releasing 3D printed poly(acrylic acid)/F127/cellulose nanocrystal hydrogels

Abstract

3D printing has been increasingly proposed to produce smart hydrogels for biomedical applications, considering their similarity to tissue structure and drug delivery capacity. Herein, we describe an innovative method for the 3D-printing of semi-interpenetrating (semi-IPN) hydrogel networks made up of poly(acrylic acid)/Pluronic F127/cellulose nanocrystals (PAA/F127/CNC) in the absence of organic solvents. 3D printed PAA/F127/CNC hydrogels were obtained by Digital Light Processing (DLP) and displayed a dense morphology, modified by CNC concentrations above 0.25 wt%, as revealed by SEM micrographs. TEM analysis revealed the presence of F127 micelles in a partial long-range order arrangement in the photopolymerized PAA/F127/CNC hydrogels, which conferred compressibility to the material. 3D printed PAA/F127/CNC hydrogels charged with the NO-donor S-nitrosoglutathione (GSNO) showed dose-response NO release profiles upon hydration, with NO release initial rates increase due to the presence of CNCs. Therefore, 3D-printed PAA/F127/CNC/GSNO hydrogels may serve as a versatile soft biomaterial for NO delivery in biomedical applications.

Introduction

In recent years, three-dimensional (3D) printing has shown great potential for the fabrication of medical devices[83,84] and tissue scaffolds[52,85] based on hydrogels. However, the balance between printing quality and material properties remains a great challenge and relies strongly on composition and printing technique.[86] In this regard, several 3D printing methods are reported for the synthesis of hydrogels, *e.g.* extrusion-based,[50,52,85] inkjet-based[87] and photopolymerization-based 3D printing[83,86,88]. The latter depend on selective exposure of monomeric mixtures (*i.e.* resins) to light. In digital light processing (DLP) 3D printers, the polymer is cured by dynamic patterning of layers, with the aid of digital micromirror devices (DMD) capable of moving and directing the light in the form of 2D patterns ("slices").[89] DLP printing offers advantages when compared to other photopolymerization techniques, such as reduced building times, less influence from O_2 inhibition and high resolution.[46]

Hydrogels comprised of poly(acrylic acid) (PAA) fulfil the requirements for DLP printing of biomedical devices, since the acrylic acid monomers are easily photoinitiated. PAA is a highly hydrophilic and pH-responsive polymer, due to pendant carboxylic groups. Additionally, it is biocompatible,[8,90] which is attractive for smart drug delivery, but results in fragile and brittle assembles.[91] The preparation of semi-interpenetrating (semi-IPN) polymer networks is a promising strategy to deal with the poor mechanical properties of PAA hydrogels. In these materials, PAA forms a crosslinked network, where linear or branched polymers are non-covalently dispersed.[1] PAA hydrogels produced in the presence of Pluronic F127 (F127) have been extensively studied.[10,30,79] F127 is a triblock copolymer of poly(ethylene oxide)-b-poly(propylene oxide)-b-poly(ethylene oxide) (PEO-PPO-PPO), capable of micellization due to dehydration and hydrophobic interactions of PPO chain segments, thus resulting in a PPO core surrounded by a PEO shell. Furthermore, the hard-sphere interactions of F127 micelles lead to liquid crystalline mesophases, depending on the temperature and concentration.[23–25] The enclosure of these F127 micellar structures within the hydrogel can provide multiple non-covalent interactions with the crosslinked PAA network, enhancing the mechanical performance.

Regarding the 3D printing of PAA-based hydrogels containing F127, Viana *et. al.*[92,93] presented a rheological study to compatibilize mixtures of AA and F127, resulting in extrudable gels, which can be further exposed to light, in order to obtain crosslinked PAA. The approach was promising considering the possibility to use non-expensive, homemade

printing devices but was unable to achieve the high resolution of DLP printing. Moreover, the work from Dutta *et al.*[54] shows a SLA printing methodology to copolymerize F127-dimethacrylate with acrylic acid. Despite the high resolution achieved, characteristic of a photopolymerization-based printing, the method used for F127 functionalization required a metal catalyst and non-friendly solvents.

Recently, considerable effort has been made towards the synthesis of semi-IPN hydrogels containing cellulose nanocrystals (CNCs).[20,37] Briefly, CNCs are rod-like particles (diameter *ca.* 5-20 nm and length 100-200 nm) derived in general from cellulose hydrolysis.[34] Due to their impressive mechanical properties and hydrophilicity, they are considered promising filler agents. Furthermore, CNCs are renewable, sustainable, biocompatible, and low-cost materials.[31,94] These features are useful to modulate the physico-chemical properties of semi-IPN PAA hydrogels for biomedical applications and the compatibilization of both CNC and F127 in a PAA-based hydrogel remains a novel approach up to now.

In previous works from our group, hydrogels have been applied as a delivery platform for nitric oxide (NO).[30,95] This small, free-radical molecule has a central role in vascular tonus and mediates wound healing, platelet adhesion, as well as angiogenesis.[62,96] These properties can be explored in the fabrication of medical devices, envisioned for improved host-guest interactions in implants and tissue scaffolds.

So far, very few works have applied 3D printing to obtain NO-releasing constructs, however, in a nozzle-based approach.[97] Consequently, the development of both new printing methodologies and materials are necessary and could represent a great progress in regenerative and personalized medicine. With this aim, we developed DLP 3D-printed semi-IPN hybrid hydrogels made up of poly(acrylic acid) (PAA) and F127, containing physically entrapped CNC (PAA/F127/CNC) for local NO release from S-nitrosoglutathione (GSNO), incorporated through absorption from solution. The PAA/F127/CNC hydrogels were formulated through an innovative approach, in the presence of CNC concentrations ranging from 0 to 1 wt%. All compositions were printable in a DLP printer. Hydrogel morphology, swelling and compression properties were investigated. Finally, NO release profiles were characterized for PAA/F127/CNC/GSNO hydrogels.

Experimental procedure

Materials

Pluronic® F127 (PEO_{99}-PPO_{65}-PEO_{99}) of 12,600 g mol^{-1} nominal molar mass, acrylic acid (AA, 99%, containing 200 ppm MEHQ inhibitor), Irgacure® 819 – phenylbis(2,4,6-trimethylbenozoylphosphine) oxide (97%), SUDAN I - 1-(phenyldiazenyl)naphthalen-2-ol (≥95 %), sodium phosphate monobasic monohydrate ($NaH_2PO_4.H_2O$, ≥98%), sodium phosphate dibasic anhydrous (Na_2HPO_4, ≥98%); potassium chloride (KCl, ≥99.0%), sodium chloride (NaCl, ≥ 99.0%), L-glutathione reduced (GSH, ≥ 98.0%) and sodium nitrite ($NaNO_2$, ≥ 99%) were acquired from Sigma Aldrich (St. Louis – MI, USA). N,N'-methylenebisacrylamide – MBA (96%) was obtained from Acros Organics (Geel, BE). Hydrochloric acid (37%) was purchased from Synth (Diadema – SP, BR). Reagents were used without previous purification steps. Uranyl acetate solution (4 wt/vol%), used for negative staining of cryosectioned hydrogels, was kindly provided by the Brazilian Center for Research in Energy and Materials – CNPEM (Campinas – SP, BR). Cellulose nanocrystals – CNCs (nominal width: 5-20 nm; length: 150-200 nm) were acquired as an aqueous gel (11.5-12.5 wt% CNCs) from the University of Maine (Orono – ME, USA). All the solutions were prepared with deionized water from a Direct-Q 3 UV system (Merck Millipore – Burlington, MA, USA).

Preparation of 3D-printable resins

Firstly, F127 was solubilized in water to form a 35 wt% solution, following the cold method, as described elsewhere.[26] As an example, 35 g F127 were added to 65 g cold DI water under stirring and stored at 4°C until complete solubilization. CNCs were dialyzed in DI water for 5 days to remove salts and preservatives, resulting in a suspension with 8.3 wt% CNCs, measured after 24 h under vacuum drying.

To prepare the 3D-printable resins, as depicted in **Fig. S1**, the required amounts of water and CNC suspension were mechanically mixed and then the cold F127 solution was added, resulting in a 20 wt% final concentration of F127 relative to total resin feed. Simultaneously, MBA (crosslinker), Irgacure 819 (photoinitiator) and SUDAN I (photoblocker) were directly added to the monomer (AA) at room temperature, and vigorously mixed with the F127-CNC suspension in an ice bath. The printable resin was kept protected from light and stored at 4 °C to avoid degradation.

The required amounts of each component in the resin formulations are summarized in **Table 7**. PAA/F127/CNC X formulations were named after the relative percentage of CNCs in the resin: 0 wt%; 0.25 wt%; 0.5 wt%; 0.75 wt% and 1 wt%. Hydrogels were produced in the presence of a 150:1 monomer:crosslinker (AA:BIS) molar ratio, except for samples prepared for TEM and SAXS experiments, where AA:MBA = 30:1. In this case, samples were coded as AB30, to distinguish them from the original formulations.

Table 7. Component concentrations of the 3D-printable resins containing increasing amounts of CNCs.

Hydrogel	AA (% wt.)	MBA (% wt.)	Irgacure (% wt.)	F127 (% wt.)	SUDAN (% wt.)	CNC (% wt.)
PAA/F127/CNC0	28.8	0.4	0.08	20	0.01	0
PAA/F127/CNC0.25	28.8	0.4	0.08	20	0.01	0.25
PAA/F127/CNC0.5	28.8	0.4	0.08	20	0.01	0.5
PAA/F127/CNC0.75	28.8	0.4	0.08	20	0.01	0.75
PAA/F127/CNC1	28.8	0.4	0.08	20	0.01	1
PAA/F127/CNC0/AB30*	28.8	2.1	0.02	20	0	0
PAA/F127/CNC1/AB30*	28.8	2.1	0.02	20	0	1

*Samples used only for structural analyses in TEM and SAXS experiments.

DLP 3D printing of hydrogels

3D modelling was performed using Blender 2.80 source software (Blender Foundation, Amsterdam – NE). The printing process was carried out at 25 °C in a DLP-printer MoonRay D75 (SprintRay, Los Angeles – CA, USA) equipped with a LED projector with 405 nm emission wavelength. The maximum resolution on the xy-plane was 75 µm, according to the manufacturer specifications. The printing step size was set on 100 µm.

For printing, *ca.* 100 mL of a previously prepared printable resin were transferred to the printer tank and the system was configured with a pre-determined set of parameters, such as exposure time, light intensity and interval between irradiations, originally designed for NextDent® Ortho IBT resins. After printing, hydrogels were removed from the printing head and rinsed several times with ethanol and water to remove uncured superficial resin.

Subsequently, hydrogels were immersed in water and were UV post-cured in a photocuring oven (LabFlo, S. Bernardo do Campo – SP, BR) equipped with a 70 W LED source for 6 min. Hydrogel samples designed for NO release experiments were extracted in *ca*. 500 mL ethanol for 5 days and in the same volume of water for 2 days under stirring. The solvent was daily changed. After washing, hydrogels were vacuum dried and stored. Finally, samples were inspected under an optical microscope (Nikon 50i, Minato - Tokyo, JP).

Fourier Transformed Infrared Spectroscopy (FTIR)

FTIR spectra of previously dried hydrogels and resin components (AA, MBA, F127, CNCs) were obtained in a 630 FTIR spectrophotometer (Agilent Cary, Santa Clara – CA, USA) in the 4000-400 cm^{-1} range and ATR mode, by depositing the samples directly over the ZnSe crystal.

Scanning Electron Microscopy (SEM)

Surface and cross-sectional morphologies of dried PAA/F127/CNC hydrogels were investigated using a Quanta FEG 250 microscope (FEI Company, Hillsboro – OR, USA) at a10 kV acceleration voltage. For cross-sectional imaging, hydrogel samples were frozen in liquid N_2 and then cryo-fractured. Subsequently, samples were mounted onto brass stubs and coated with iridium in a high vacuum MED 020 coating system (BAL-TEC, Balzers, LI), operating at 13.8 mA, for 180 s.

Cryogenic Transmission Electron Microscopy (Cryo-TEM)

The long-range ordering of F127 micelles was investigated by Cryo-TEM in a TEM-JEOL 1400 (JEOL Instruments, Akishima – Tokyo, JP) at 120 kV acceleration voltage. Images were recorded in a OneView camera system (GATAN, Pleasanton – CA, USA). F127 20 wt% solution and PAA/F127/CNC0/AB30 resin were deposited on lacey carbon grids (300 mesh, TED PELLA, INC., Redding, CA, USA) previously glow discharged, at 15 mA for 25 s in a PELCO EasiGlow device (TED PELLA). Sample preparation was performed in a Vitrobot equipment (Thermo Fisher Scientific, Hillsboro – OR, USA), according to the following procedure: 2 µL of sample were deposited onto the grid at 15 ºC and 100% water saturation. The excess of liquid was removed by double blotting (blot force = -2, time per blot

= 1.5 s). Immediately, temperature was elevated to 30 ºC during 300 s drain time. In sequence, grids were plunged into liquid ethane for vitrification and stored in liquid N_2 before transference to the thermalized microscope sample holder.

Transmission Electron Microscopy (TEM)

Hydrogels (PAA/F127/CNC0/AB30 and PAA/F127/CNC1/AB30) were sectioned in a Leica EM UC/FC6 ultramicrotome (Leica Microsystems, Wetzlar – HE, DE) and mounted onto copper grids (TED PELLA, INC., Redding - CA, US). Subsequently, sections were negatively stained. For this, a 4 wt/vol% uranyl acetate stock solution was diluted to 2 wt/vol% and applied at both sides of the grid for 30 s. Imaging was performed in a Libra 120 microscope (Carl Zeiss, Oberkochen – BW, DE), operating at a 80 kV acceleration voltage.

Small Angle X-Ray Scattering (SAXS)

SAXS experiments were performed at the SAXS1 beam line of the Brazilian Synchrotron Light Laboratory (LNLS – CNPEM, Campinas – SP, BR), operating at 8 keV energy and 1.48 Å wavelength, equipped with a 2D detector Pilatus 300k (Dectris, Baden – CH). Silver behenate was used as calibration standard for sample-detector distance, which was equal to 1 m, resulting in a 0.15 - 5 nm^{-1} q range. A 20 wt% F127 solution, as well as a PAA/F127/CNC0/AB30 3D-printable resin were transferred to transmission cells covered with mica at both sides. Dry hydrogels produced without CNCs (PAA/F127/CNC0 and PAA/F127/CNC0/AB30) as well as hydrogels produced in the presence of 1 wt% CNCs (PAA/F127/CNC1 and PAA/F127/CNC1/AB30) were cut in small blocks and inserted in a sample holder between two Kapton tapes. Data were processed for background correction and the resulting 2D patterns were radially averaged and converted to I(q) versus q scattering patterns.

Hydrogel Swelling

Hydrogel swelling analysis was carried out on printed discs with ca. 3 mm height and 6 mm diameter immersed in PBS buffer (pH = 7.4, 0.01 M) at 37 ºC during 72 h. Each hydrogel was immersed in a volume at least 20-fold higher than the initial hydrogel mass and were weighted in regular time intervals after gently wiping the surface with qualitative filter paper. The buffer solution was replaced on a daily basis. The swelling (S) of hydrogels,

expressed as weight ratio of absorbed water per hydrogel weight (g/g), was obtained according to the **Eq. 3**:

$$S = \frac{W_s - W_d}{W_d} = kt^n \text{ (**Equation 3**)}$$

where W_s represents the weight of the swollen hydrogel at time t and W_d the weight of the dried hydrogel at t=0.

The swelling ratio can be used to study the mechanism of solvent diffusion through the polymeric matrix, according to a power law, where k is a constant related to the solvent-hydrogel system, and n represents the diffusional exponent.[38] To obtain the n values, **Eq. 3** was linearized, resulting in **Eq. 4**, where C is a constant, equivalent to $n \ln k$.

$$\ln S = C + n \ln t \text{ (**Equation 4**)}$$

The swelling kinetics of hydrogels was discussed in terms of a second-order process,[98] according to the **Eq. 5**.

$$\frac{dS}{dt} = k_s\left(S_{eq} - S\right)^2 \text{ (**Equation 5**)}$$

where k_s represents the swelling rate constant, S_{eq} the equilibrium swelling ratio and S the swelling at time t. This differential equation can be integrated, resulting in a linear equation in terms of time, as shown by **Eq. 6**.

$$\frac{t}{S} = A + Bt \text{ (**Equation 6**)}$$

The intercept in a plot of t/S versus t, $= \frac{1}{k_s S_{eq}^2} = \frac{1}{\left(\frac{dS}{dt}\right)_0}$, represents the reciprocal of the initial swelling rate, and the slope $B = \frac{1}{S_{eq}}$ is the reverse of equilibrium swelling ratio.

Compression tests

The compression of PAA/F127/CNC 3D printed hydrogels was performed in a TA.XT Plus Texture Analyzer (Stable Microsystems, Godalming – SRY, UK) at 25 ºC. Hydrogels were previously printed as cylinder probes with 10 mm diameter and ca. 8 mm height and kept at 4 ºC in closed vials under saturated water atmosphere to prevent drying. Prior to analysis, the vials were equilibrated at room temperature for 72 h. For this analysis, four compression-decompression cycles were performed in triplicate with a 5 kg load cell at a 0.1 mm s^{-1} compression rate and 50% maximum compression. The Young's moduli of PAA/F127/CNC hydrogels were calculated as the slope of stress versus strain ($\epsilon=|\Delta L|/L$) of the initial linear section of the compression curves. The analyzed samples were vacuum dried for 72 h, resulting in cylinders with ca. 8 mm diameter and 6 mm height, which were subjected afterwards to the same analysis conditions.

Chemiluminescence nitric oxide release detection

The synthesis of GSNO was adapted from Seabra *et al.*[99] Briefly, equimolar amounts of GSH and $NaNO_2$ (ca. 0.6 mol L^{-1}) in acidic medium (0.5 M HCl) reacted under mixing for 90 s in an ice bath, covered on aluminium foil. GSNO was precipitated into five-fold excess acetone, vacuum filtered and lyophilized. The resulting GSNO was 95% pure, as quantified by liquid chromatography (UPLC Acquity, Waters, Millford – MA, USA).

Discs of PAA/F127CNC0 and PAA/F127CNC0.25 hydrogels ($\varnothing = 6$ mm, $h = 1$ mm) were impregnated with GSNO in 5 mM, 10 mM and 20 mM aqueous solutions at room temperature for 24 h. Hydrogels were afterwards rinsed with water, freeze-dried and stored at -20 ºC protected from light and humidity in a desiccator. The total GSNO load in the hydrogels was measured by chemiluminescence in a NO analyzer (NOA, Sievers 280i, GE Analytical Instruments, Boulder – CO, USA), under 6.0 psig (ca. 310 torr) of O_2 and 8.0 torr of N_2, in accordance to the ascorbate method.[100] In brief, hydrogels were immersed in 160 mM ascorbic acid solution prepared in basic medium (0.2 M NaOH) and exposed to light from a 780 lumen LED source (LMI-6000, Dolan-Jenner Industries, Boxborough – MA, USA). Results were expressed in units of nmol of GSNO per mass of dry hydrogel (nmol g^{-1}).

The NO release profiles were acquired using the NOA, operating at the same parameters in absence of light. The hydrogel discs loaded with GSNO were placed inside of the NOA reaction flask containing 10 mL of PBS buffer (0.01 M, pH 7.4), thermalized at 37

°C. Hydrogels were immersed for 180 min and the chemiluminescent signal was converted to NO content after calibration with known amounts of $NaNO_2$. The resulting real-time NO release profiles were integrated and normalized to the initial hydrogel mass to obtain cumulative NO release profiles, expressed as nmol of NO per mass of hydrogel (nmol g^{-1}).

Data processing and statistical analysis

In this work, swelling experiments, compression tests, GSNO load measurements, as well as NO release profiles were performed in triplicate and results were expressed as mean values and standard deviations in appropriate units. Origin® 8.1 software (OriginLab Corporation, Northampton, Massachusetts, USA) was used for data plotting, linear curve fittings and statistical analysis. One-way ANOVA tests were employed for mean comparisons, according to Tukey's method at significance level of 95% ($p<0.05$).

Results and Discussion

The 3D-printable resins were prepared in a two-step process, as illustrated in **Fig. S1**. The first step concerned the mixing and homogenization of F127 and CNC suspensions. This previous dissolution was carried out to avoid the formation of CNC aggregates, but limited the maximum CNC concentration to 1 wt% in the final mixtures. Since F127 solutions undergo temperature-responsive gelation above 16 wt% at 25 °C,[101,102] the dispersion of the components was carried out in an ice bath, by mixing the required amounts of water and CNCs, and then adding the cold F127 solution.

Here, we describe a novel method to prepare PAA/F127/CNC hydrogels, where MBA, Irgacure 819 (photoinitiator) and SUDAN I (photoblocker) were directly dissolved in the acrylic acid monomer, at room temperature. The high concentration of F127 in the formulations prevented the use of organic solvents to solubilize the photoinitiator and the photoblocker, which are poorly water-soluble. The monomer solution was finally mixed at low temperatures with a previously prepared suspension of non-functionalized F127 and CNC, resulting in a 3D-printable resin.

During printing, Irgacure 819 undergoes unimolecular cleavage, yielding free-radicals in the resin bulk.[103] These radicals initiate the polymerization reaction of AA and MBA vinyl groups and then the reaction is propagated. Since polymerization occurs in the presence of

non-crosslinked entities, such as F127 and CNCs, a semi-IPN hydrogel network is expected to be formed, as depicted in **Fig. 20**.

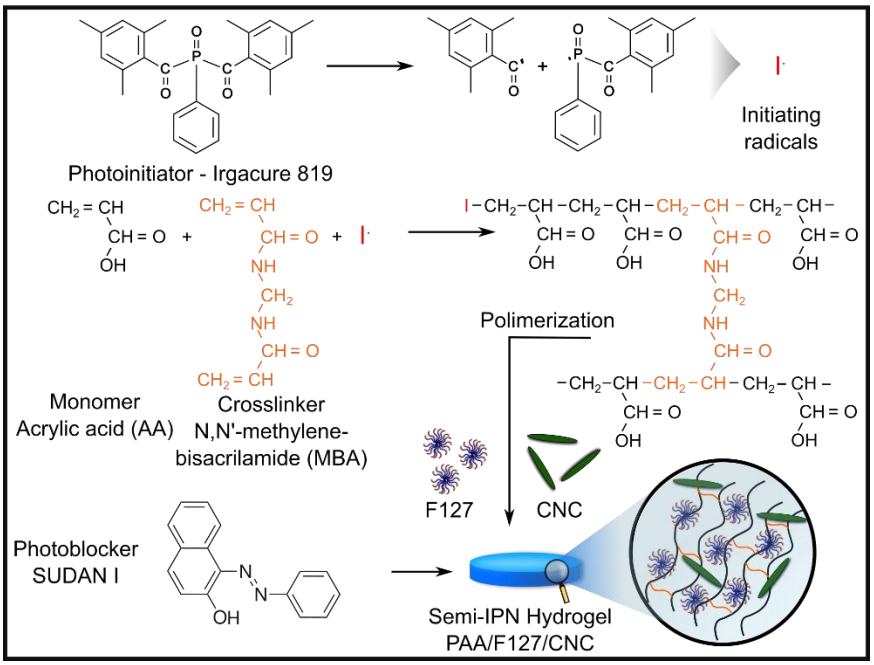

Figure 20. Proposed reactions of PAA crosslinking and formation of PAA/F127/CNC hydrogels during 3D DLP printing.

To print PAA/F127/CNC hydrogels, parameters such as light intensity, time of exposure and step size were restrained by manufacturer. In this sense, the resins were adapted by controlling the relative proportions of photoinitiator and photoblocker. This balance was fundamental to avoid overcuring, when light penetrates deeper than the step size of printing, increasing layer thickness beyond programmed boundaries.[57] Benjamin *et al.*[86] reported a systematic approach for resin formulation, where the curing depth was studied as a function of the photoblocker concentration. The curing depth controls not only the limits of each printed layer, but also if the next layer can adhere to the latter. One suggestion of their study is to use the highest possible photoblocker concentration and vary the layer thickness, in order to avoid the obstruction of voids in the 3D printed parts. Considering this, the 3D-printable resins were produced with CNC contents in a range between 0 wt% and 1 wt% (**Table 7**). It was found that a 5:1 photoinitiator:photoblocker molar proportion, with a 100 µm layer thickness,

enabled high quality printings even under the highest CNC concentration, which caused intense light scattering due to the Tyndall effect.

Additionally, PAA/F127/CNC hydrogels were designed in different shapes to proof the effectiveness of the printing methodology and were printed horizontally with respect to the printing head, preserving internal channels in the 3D models (**Fig. S2**).

Fourier Transformed Infrared Spectroscopy (FTIR)

To assess the polymerization of the resin formulations, FTIR spectra of the printed hydrogels were compared to the components of the polymerizable resins, as shown in **Fig. 21**.

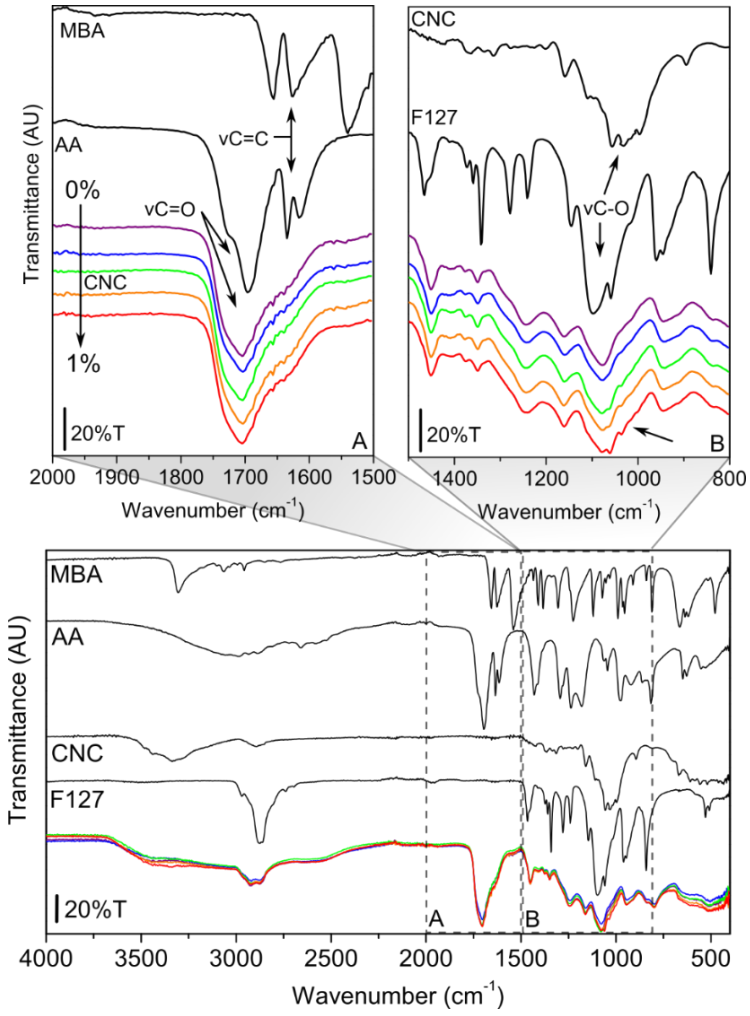

Figure 21. FTIR spectra of PAA/F127/CNC hydrogels concentrations and corresponding components. Range: (A) 2000 cm^{-1} – 1500 cm^{-1}; (B) 1500 cm^{-1} – 800 cm^{-1}. Hydrogels were ordered by decreasing CNC concentration, as indicated in (A).

The AA FTIR spectrum (**Fig. 21A**) shows in the 2000 cm^{-1} and 1500 cm^{-1} range bands centered at 1696 cm^{-1} and 1632 cm^{-1}, assigned to C=O and C=C stretching vibrations, respectively.[73,74] The corresponding bands in the MBA FTIR spectrum were found centered at 1655 cm^{-1} and 1627 cm^{-1}.[75] For all hydrogel compositions, the bands assigned to C=O stretching were shifted to a higher wavelength (1703 cm^{-1}) in relation to that of AA and MBA. Additionally, the band assigned to the carbon double bonds vanished, indicating that curing was effective. The FTIR spectrum of F127 (**Fig. 21B**) shows an intense band at 1090 cm^{-1}, assigned to the -C-O stretching vibration of the PEO and PPO polyether blocks.[76] This band was found at a lower wavelength, 1077 cm^{-1} in hydrogel spectra. The observation of shifts rather than disappearance of bands supports the hypothesis that F127 interacts with the PAA network through hydrogen bonding, suggesting that a semi-IPN network was formed.[79] Lastly, the FTIR spectrum of dried CNCs (**Fig. 21B**) shows the characteristic C-O vibration at 1056 cm^{-1}. This band becomes visible by increasing the CNC content in the hydrogels, suggesting that the CNC entrapment was successful.

Scanning Electron Microscopy (SEM)

The 3D printed hydrogels were imaged in a scanning electron microscope and then compared with their models to evaluate the printing fidelity, as shown in **Fig. 22**.

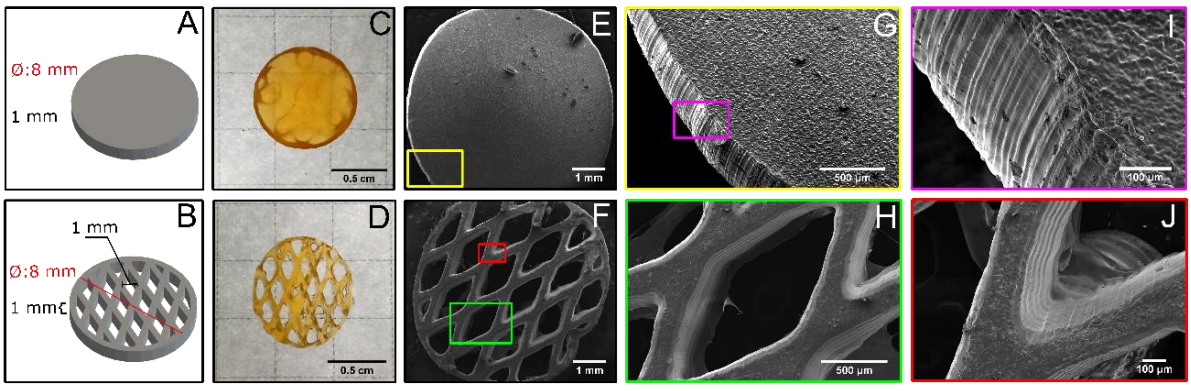

Figure 22. 3D-printable discs developed for NO delivery: (**A**) Disc and (**B**) net. Photographs of the as-printed hydrogels: (**C**) disc and (**D**) net. Representative SEM micrographs of a PAA/F127/CNC0 (**E**) disc and (**F**) net. (**G** and **I**) show magnifications of the disc and (**H** and **J**) respective magnifications of the hydrogel net.

Dense discs and discs containing regularly sized voids (nets) were modelled as exemplified in **Fig. 22A** and **Fig. 22B**, respectively. Photographs of hydrogels printed according to these models (**Fig. 22C** and **Fig. 22D**) show that PAA/F127/CNC constructs were obtained with good fidelity to their originals. A dense PAA/F127/CNC0 disc, such as the one displayed in **Fig. 22E**, exhibited a 6 mm diameter in the dry state, which represented shrinkage of ca. 25% with respect to the model. A close look at the top (**Fig. 22G**) and at the lateral side of the disc (**Fig. 22I**) revealed regular surface patterns. Since these surfaces were not directly attached to the printing head, their features were assigned to the micromirror array (DMD), which is responsible for generating the patterns of each printed layer. The DMD controls the pixel size of the printings and the resolution of the DLP printer over the xy plane,[89] which is of 75 µm for the printer used in this work. Moreover, the printed net micrograph presented in **Fig. 22F** indicates that the method enables high quality hydrogel printing, resulting in widths as low as 180 µm for the magnified structures in **Fig. 22H** and **Fig. 22J**. The latter also presents a ridged pattern, which is characteristic of the layered nature of the DLP printing.

The internal morphology of the 3D-printed and vacuum dried PAA/F127/CNC hydrogels was investigated without any washing step. Representative SEM cross-section micrographs obtained by cryofracturing are shown in **Fig. 23**.

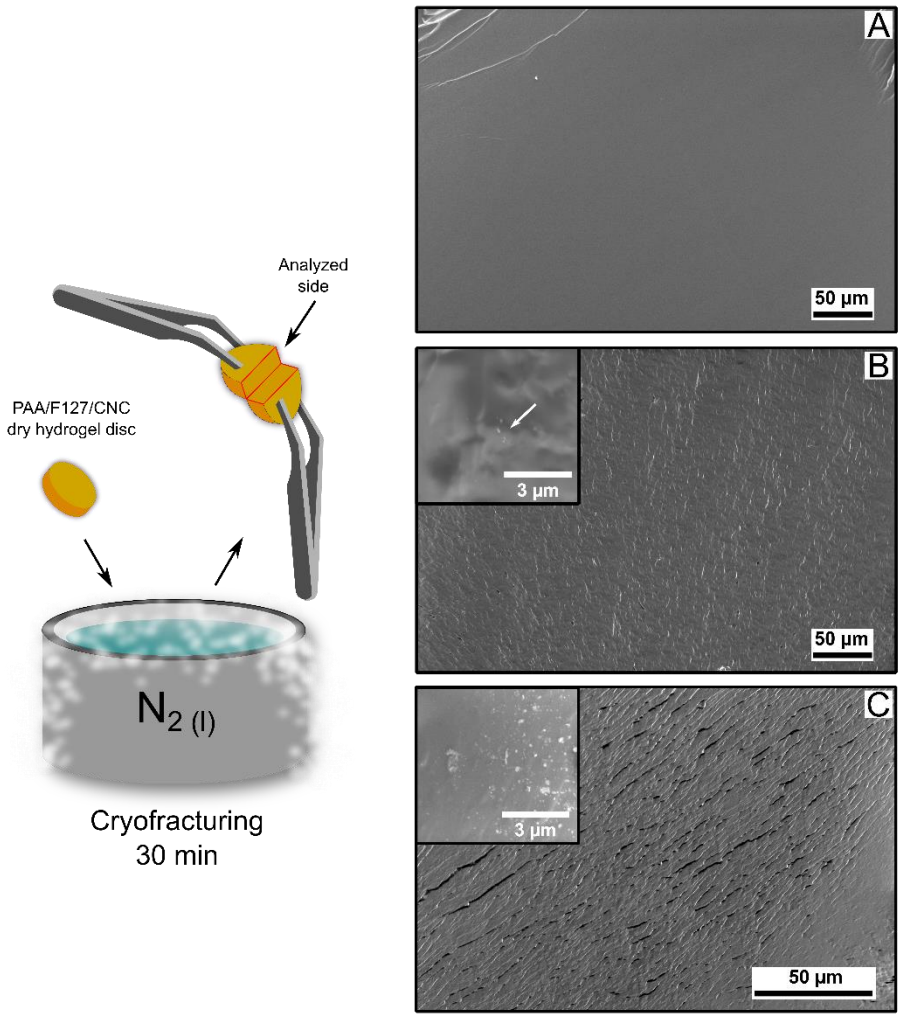

Figure 23. Schematic representation of the hydrogel cryofracture process and **c**ross-sectional SEM micrographs of the 3D printed PAA/F127/CNC hydrogels. (A) PAA/F127/CNC0, (B) PAA/F127/CNC0.25 and (C) PAA/F127/CNC1. The inset micrographs in (B) and (C) highlight occurrences of CNC aggregates.

The images reveal uniform cross-sections without pores, which are characteristic of dense materials. Moreover, no evidence of tearing was observed, suggesting that the printable formulations generated well adhered layers during the printing process. However, the introduction of CNCs seems to influence hydrogel morphology. While PAA/F127/CNC0 hydrogels (**Fig. 23A**) exhibited smooth cross-sections, PAA/F127/CNC0.25 (**Fig. 23B**) showed roughness, which was even more pronounced in PAA/F127/CNC1 hydrogels (**Fig. 23C**). These observations suggest that high CNC contents may lead to more brittle hydrogels,

possibly due to CNC aggregation. Aggregates could be observed in rare spots in PAA/F127/CNC0.25 but were abundant in PAA/F127/CNC1 cross-sections, as highlighted by the white dots in the inset micrographs. Therefore, the mechanical reinforcement expected by CNCs in PAA/F127/CNC hydrogels is possibly restricted to a low CNC concentration range, which may be expanded by more efficient homogenization methods.

Cryogenic Transmission Electron Microscopy (Cryo-TEM)

In this work, printable solutions containing 20 wt% F127 were prepared aiming at attaining a supramolecular structure of packed F127 micelles entrapped in the hydrogel matrix after 3D printing. To investigate the supramolecular structure during the printing process, cryo-TEM micrographs were taken (**Fig. 24A, Fig. 24B**).

Fig. 24A shows a cryo-TEM micrograph of pure 20 wt% F127 hydrogel. A 13 nm interplanar spacing, assigned to the periodic ordering of hydrophobic PPO cores,[104] can be measured throughout the imaged area. **Fig. 24B** shows that, in the printable resin containing the same F127 concentration, F127 micelles were partially preserved before polymerization, forming disordered domains (yellow contours). Therefore, it can be proposed that the intermolecular interactions between F127 unimers and the resin components affected the self-assembling of the micelles.

Transmission Electron Microscopy (TEM)

Fig. 24C depicts the TEM micrograph of a cryo-ultramicrotomed cross-section of the PAA/F127/CNC0/AB30 hydrogel. Uranyl negative staining of the samples revealed white dots, which are characteristic of F127 micelles, with sizes in the 14±2 nm range. However, a long-range ordering was absent. The same behavior was observed for PAA/F127/CNC1/AB30 hydrogels, as shown in **Fig. 24D**. F127 micelles remained dispersed in the polymer matrix, presenting a 18±3 nm diameter.

The preservation of F127 micelles inside the PAA hydrogel matrix was expected, according to Champeau *et al*.[30] Their work revealed, through SAXS analyses, a partial long-order retention of micelles in dry hydrogel samples, produced via thermally activated polymerization

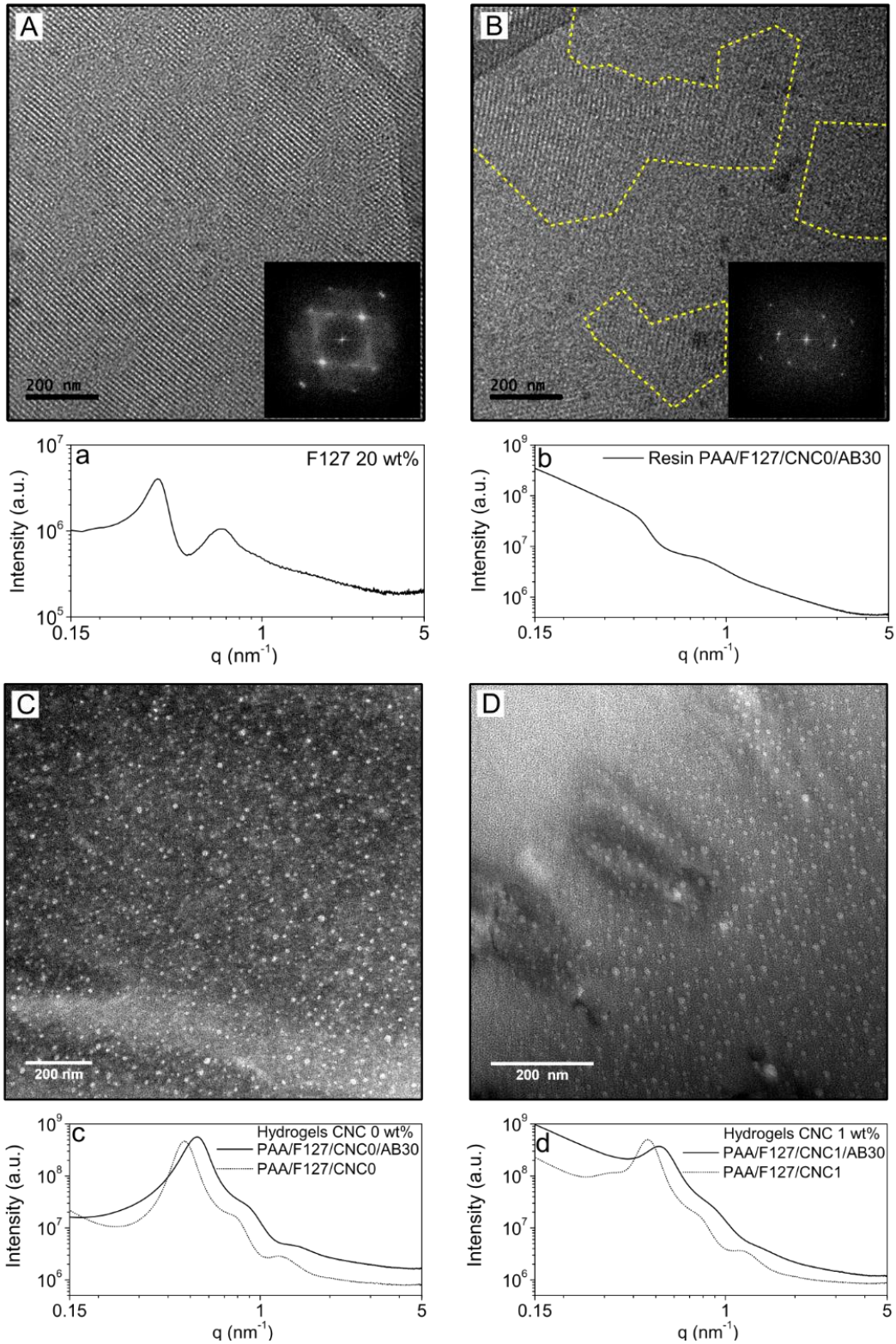

Figure 24. Investigation of F127 micellization in resin and photopolymerized PAA/F127/CNC hydrogels. Cryo-TEM micrographs of (A) 20 wt% F127 solution and (B) PAA/F127/CNC0/AB30 3D printable resin. Insets in (A) and (B) depict the respective fast Fourier transform (FFT). The yellow contour in (B) highlights ordered F127 domains. TEM

micrographs of (C) PAA/F127/CNC0/AB30 and (D) PAA/F127/CNC1/AB30 hydrogels. SAXS profiles are represented below the corresponding micrographs: (a) 20 wt% F127, (b) PAA/F127/CNC0/AB30 resin, (c) PAA/F127/CNC0/AB30 hydrogel (solid) and PAA/F127/CNC0 hydrogel (dots) (d) PAA/F127/CNC1/AB30 hydrogel (solid) and PAA/F127/CNC1 hydrogel (dots).

Small Angle X-ray Scattering (SAXS)

TEM micrographs provide valuable information on the structural hierarchy of the F127 micelles in the hydrogels. However, these images represent only a small portion of the sample and techniques such as SAXS render averaged and complementary results. A SAXS pattern of a 20 wt% F127 solution at 25 ºC is shown in **Fig. 24a**. Two peaks at $q_1 = 0.354$ nm^{-1} and $q_2 = 0.67$ nm^{-1} were observed. Their relative positions correspond to a $\sqrt{3}$: $\sqrt{11}$ ratio, which can be assigned to the (111) and (311) reflections of a face-centered cubic (FCC) packing. The observed signals were broad due to incomplete gelation process or even to non-uniform structures. Additionally, a 30.7 nm lattice parameter calculated for this structure, according to the equation $a_{FCC} = 2\pi\sqrt{3}/q_1$, was consistent with other literature reports.[25,30]

The SAXS profile obtained before polymerization of a PAA/F127/CNC0/AB30 resin (**Fig. 24b**) indicates retention of the partial long-order observed in the cryo-TEM micrographs, by showing two broad shoulders centered at $q_1 \sim 0.42$ nm^{-1} and $q_2 \sim 0.77$ nm^{-1}. The shift in signals corresponds to a decrease in the lattice parameter to 26.0 nm, which may occur due to the interaction of AA with F127 polar and nonpolar blocks, inducing a change in gelation process. The work reported by Ivanova *et al.*[105] shows similar results for F127 in the presence of ethanol or propylene glycol, and attributes this effect to the swelling of both PPO and PEO blocks by the glycols, which can participate in the micelle-solvent interface formation.

Fig. 24c shows a SAXS profile obtained for the polymerized PAA/F127/CNC0/AB30 hydrogel sample (**solid line**), which presents two overlapping peaks, followed by another broad peak at higher q values. These results suggest the partial retention of the F127 long-range ordering. In this sample, q_1 shifts to 0.53 nm^{-1} resulting in a 20.4 nm lattice parameter value. By using a lower proportion of the MBA crosslinking agent (PAA/F127/CNC0, **dotted line**), the SAXS profile shifted towards lower q values ($q_1 = 0.48$ nm^{-1}), reflecting an increase in lattice parameter to 22.9 nm. The changes in F127 lattice parameter are reasonable, since

F127 concentration is increased during hydrogel drying and photopolymerization induces shrinkage of the polymer matrix.[103,106]

Contrastingly, SAXS peaks from hydrogels photopolymerized in the presence of 1 wt% CNC (**Fig. 24d**) were shifted to lower q values, when compared to the samples without CNC. For a PAA/F127/CNC1/AB30 hydrogel sample (**solid line**), the primary peak q_1 = 0.51 nm^{-1} corresponds to a 21.1 nm lattice parameter. Under a lower crosslinker content (PAA/F127/CNC1, **dotted line**), q_1 resulted in 0.46 nm^{-1}, with a 23.7 nm lattice parameter. This less pronounced decrease in the characteristic dimensions of F127 domains can be rationalized by a lower degree of shrinkage, possibly caused by differences in the absorbed water content in samples. Moreover, F127 PEO blocks could potentially interact with CNC surface. This strategy has been already applied to enhance CNC dispersion through PEG adsorption.[107]

Hydrogel Swelling

Swelling kinetics and mechanical behavior are key physical properties of hydrogels, which define drug delivery capacity and possible applications for these materials. In this work, the swelling behavior of the 3D printed hydrogels was characterized in PBS buffer at 37 °C and is illustrated in **Fig. 25**.

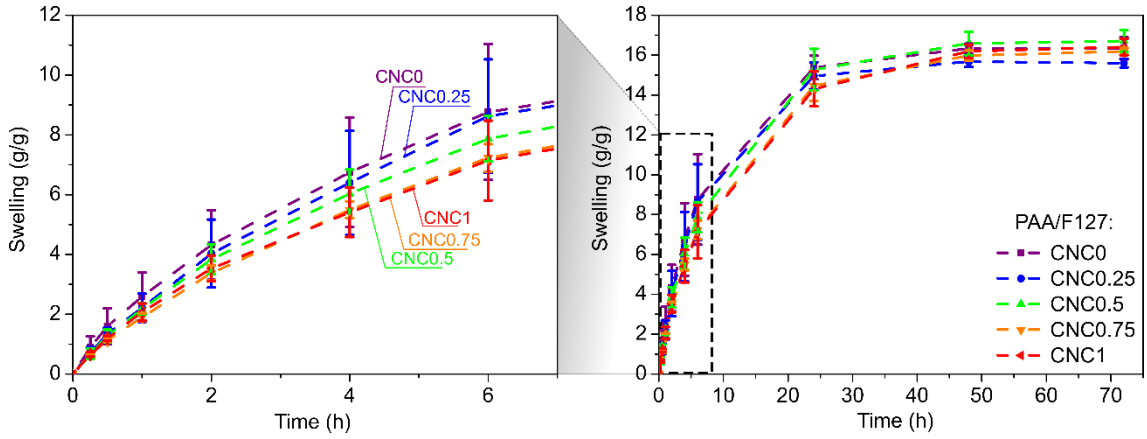

Figure 25. Swelling of 3D printed PAA/F127/CNC hydrogels with increasing CNC concentrations and measured during 72 h in PBS buffer 0.01 M, pH = 7.4, at 37 ºC. The graph on the left side shows a magnification of the first 6 h of measurement.

The analysis of swelling reveals that the PAA/F127/CNC hydrogels exhibited high water absorption in physiological conditions, with an equilibrium swelling ratio of *ca.* 16 $g_{water}/g_{hydrogel}$ (1600 wt%), typical for PAA. The hydrogel crosslinking density plays an important role in swelling, since it affects the matrix flexibility and the available volume for water diffusion across the polymer network.[108] In previous experiments (**Fig 12**), by using a five-fold increase in crosslinking agent concentration, the swelling of the hydrogels reached ca. 3 $g_{water}/g_{hydrogel}$. However, these samples showed poor mechanical properties.

Additionally, CNC incorporation in the hydrogels modified the swelling kinetics, as depicted in the magnified graph in **Fig. 25**. It was found that, as the concentration of CNCs increased, there was a slight decrease in the initial swelling rate of the 3D-printed hydrogels. However, this tendency was statistically non-significant and not maintained on swelling equilibrium. A mathematical analysis of hydrogel swelling, in accordance with a second order process, as described in **Eq. 6**, was carried out by plotting t/S versus t for different hydrogel compositions (**Fig. S3A**). The respective kinetic parameters, obtained after linear regression, are summarized in **Table S1** and support the tendency of decreasing swelling rate values upon CNC concentration increase, without apparent influence on equilibrium swelling ratios. This result was surprising, given the hydrophilic character of CNCs and the divergence of it and the results shown in Chapter 1, probably due to the differences in the AA:MBA molar ratio and the photopolymerization process, via 3D printing instead of casting and LED irradiation. Herein, the promotion of a barrier effect upon addition of CNC could be considered to explain the apparent decrease in swelling rates, due to an increase in the diffusional path of water molecules in the hydrogels.[20]

The mechanism of water diffusion through the PAA/F127/CNC hydrogels was studied using the logarithmic model shown in **Eq. 4**, by plotting ln S versus ln t (**Fig. S3B**) for each hydrogel composition. The slopes obtained by linear regression of these curves represent the diffusional exponent n, which are summarized in **Table S2**. For discs and cylinder geometries, if $n \leq 0.5$, diffusion occurs through a Fickian mechanism. If $0.5 < n \leq 1$, diffusion is non-Fickian, or anomalous.[38,109] Since n values ranged from 0.72 to 0.78 for these hydrogels, one can conclude that water diffusion through the printed hydrogels is non-Fickian. This behavior arises when the polymer relaxation rate is comparable to the rate of solvent diffusion through the hydrogel matrix,[110] and can be related to the dense hydrogel morphology.[109]

Compression tests

The mechanical properties of printed PAA/F127/CNC hydrogels were assessed by compression tests of cylinder probes, performed at 25 °C. Hydrogel samples were subjected to four loading/unloading cycles at a constant displacement rate. **Fig. 26** compares compression data for hydrogels with increasing CNC content.

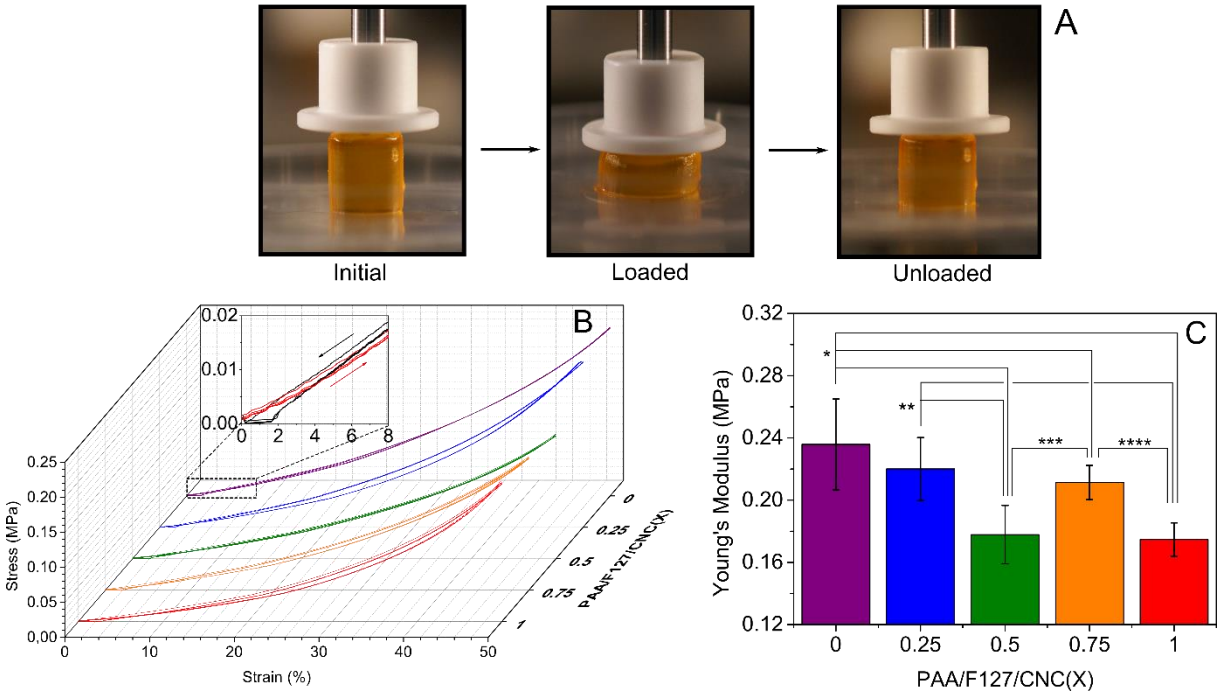

Figure 26. Compression tests of PAA/F127/CNC hydrogels. (A) Photographs of a hydrogel during a compression cycle. (B) Representative loading/unloading stress-strain curves to a maximum of 50% nominal compression per cycle. The inset shows a zoom-in view of the indicated region for the PAA/F127/CNC0 hydrogel. (C) Young's Moduli obtained from compression curves. Asterisks indicate statistically significant differences between samples, according to Tukey test with $p < 0.05$.

According to **Fig. 26A**, PAA/F127/CNC hydrogels elastically restore its original dimensions after unloading. However, **Fig. 26B** reveals the occurrence of a small hysteresis, which occurs due to a permanent deformation of the hydrogel. The area within compression and decompression curves is proportional to the mechanically dissipated energy per cycle.[111]

Consequently, the hydrogels present a viscoelastic character. Baskan and coworkers[10] crosslinked PAA with MBA in the presence of F127 and showed that the incorporation of F127 favors the formation of hysteresis due to the formation of both ionic clusters in PAA and associations between F127 chains, resulting in hydrogels capable to sustain up to 7 MPa compression at 98% strain. The Young's moduli (YM) of the 3D printed PAA/F127/CNC hydrogels were calculated from the slope of the initial linear section of the compression curves (**Fig. 26B**). The resulting mean YM values ranged from 0.16 MPa to 0.27 MPa. For reference, this range of moduli values is intermediate between typical YM of muscle tissues (0.001 – 0.003MPa)[112] and cartilages (10 – 400 MPa).[113]

Successive increases in CNC percentage led to corresponding decreases in YM values, as observed in **Fig. 26C**. This result can be mainly related to an increase in water absorption in the presence of CNC. An important aspect to be considered is that water is an efficient plasticizer of hydrophilic polymers, acting mainly in the disruption of hydrogen bonding between polymer chains.[114] Dried PAA/F127/CNC hydrogel cylinders (**Fig. S4A**) were less elastic upon compression, resulting in more pronounced hysteresis and higher YM values (**Fig. S4B**) than their hydrated counterparts. The latter were statistically equivalent for the different hydrogel compositions.

On the other hand, the addition of proper CNC amounts creates a percolation network, responsible for enhanced particle-particle interactions and mechanical properties.[31] However, high CNC concentrations show a tendency to aggregation, with the formation of CNC bundles that leads to inhomogeneities capable to affect hydrogel formation. In fact, CNC aggregates were observed in PAA/F127/CNC1 cross-sections (see **Fig. 23**) and may contribute to changes in compressive properties. Additionally, Yang *et al.*[41] reported the synthesis of injectable hydrogels based on dextran and carboxymethylcellulose (CMC) reinforced with CNCs. In their work, an increase in dynamic storage modulus (G') was observed for low CNC concentrations (below 0.375 wt%) followed by decrease in G' values, which was ascribed to a CNC steric hindrance of the cross-linking between dextran and CMC.

Chemiluminescence NO release detection

PAA/F127/CNC0 and PAA/F127/CNC0.25 hydrogels were chosen to study the influence of CNC on the NO release. PAA/F127/CNC0.25 was preferred due to its higher YM compared to hydrogels containing higher CNC contents. The NO release profiles were

characterized by chemiluminescence after impregnation with 5 mM, 10 mM and 20 mM GSNO aqueous solutions. The total GSNO load in hydrogels was obtained by accelerated NO release in the presence of ascorbate solution and light and the resulting values are displayed in **Table S3**.

According to the results shown in **Table S3**, the GSNO uptake by hydrogels depended on the initial loading concentration. However, the hydrogel composition did not affect substantially the GSNO load values. This behavior is reasonable, since impregnation is swelling controlled and the used hydrogel compositions showed very similar swelling profiles. The kinetics of NO release was analyzed by immersion of the GSNO-loaded hydrogels in PBS at physiological temperature for 180 min. The NO chemiluminescence signal was converted to NO quantities (nmol) after calibration with known amounts of NO and integrated to produce cumulative and averaged NO release profiles, shown in **Fig. 27**.

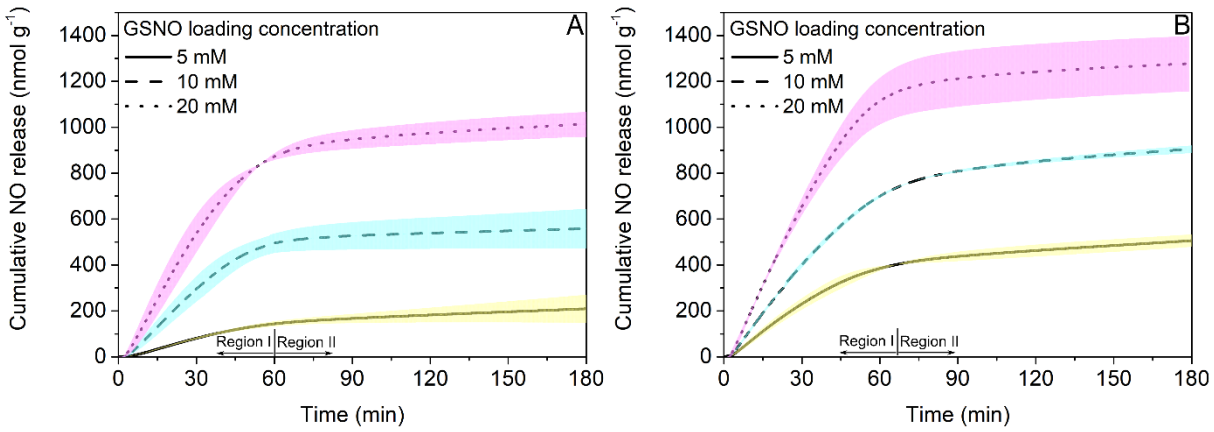

Figure 27. Cumulative profiles of NO release in PBS solution of GSNO-loaded hydrogels obtained by chemiluminescence analysis. (A) PAA/F127/CNC0/GSNO and (B) PAA/F127/CNC0.25/GSNO. Samples were impregnated with 5 mM (yellow profiles), 10 mM (cyan profiles) and 20 mM (pink profiles). The left bottom labels indicate two regions with distinct regimes of NO release.

The NO release profiles were characterized by fast releases until ca. 60 min, followed by gradual reduction in release rates until near-constant values were achieved, resulting in two distinct regions, as highlighted in both graphs. Moreover, the NO release of PAA/F127/CNC0/GSNO hydrogels (**Fig. 27A**) was slower than in PAA/F127/CNC0.25/

GSNO hydrogels (**Fig. 27B**). In order to compare the kinetics of NO release of these hydrogel compositions, the release rates were obtained by first order fitting of the cumulative profiles during the two regimes of NO release (*i.e.* first 30 min and last 90 min of analysis). The results are summarized in **Table 8**.

Table 8. NO release rates of GSNO-loaded PAA/F127/CNC0 and PAA/F127/CNC0.25 hydrogels derived from cumulative NO release profiles.

	PAA/F127/CNC0/GSNO		PAA/F127/CNC0.25/GSNO	
GSNO concentration in loading (mM)	Initial rate (nmol g^{-1} min^{-1})	Final rate (nmol g^{-1} min^{-1})	Initial rate (nmol g^{-1} min^{-1})	Final rate (nmol g^{-1} min^{-1})
5	3.1 ± 0.1	0.5 ± 0.5	8.3 ± 0.5	0.7 ± 0.1
10	11 ± 2	0.3 ± 0.3	14.7 ± 0.2	0.5 ± 0.4
20	20 ± 2	0.7 ± 0.2	24 ± 2	0.5 ± 0.1

The values of initial NO release rates confirm the tendency observed in the cumulative profiles shown in **Fig. 27** and show a dose-response, since the rate values increase as a function of the GSNO concentration during the loading procedure. The presence of CNCs increased the NO release rates, probably due to an enhanced water uptake, as CNCs possess hydrophilic character, although this result is not reflected in the swelling analysis. The NO release rates were constant after approximately 60 min of analysis. However, the signal readings were low and barely distinguishable from the baseline, resulting in rate values in the range between 0.3 nmol g^{-1} min^{-1} and 0.7 nmol g^{-1} min^{-1}, which did not depend on hydrogel composition or dose during GSNO loading. Champeau *et al.*[30] produced thermally polymerized hydrogels based on PAA and F127 employing a 60:40 PAA:F127 mass ratio, analogously as herein reported. The materials were loaded in 10 mM GSNO solutions in PBS (pH 7.4) and the NO release kinetics was studied by swelling in a humid atmosphere, resulting in NO release rates of ca. 1.25 nmol g^{-1} min^{-1}, which were even superior than the present results, thus illustrating a possibility to tune the PAA/F127/CNC hydrogel NO release kinetics by modifying the environmental conditions during GSNO loading and NO release.

The observed low NO release rate values are attractive for medical applications, since several physiological processes, such as vasodilation and wound healing, are activated by NO concentrations lying in the nanomolar range.[62] As the 3D printed PAA/F127/CNC hydrogels

present tunable, composition-dependent and dose-responsive NO release profiles, they represent a promising strategy to obtain fully customizable medical devices capable of local NO delivery, from NO releasing dermatological patches to implants envisioned for cartilage replacement (e.g. intervertebral discs, menisci, etc.). Further studies are still required to avoid material leakage from these semi-IPN hydrogels and to improve their mechanical properties, enabling long-term contact with living tissues.

Conclusions

Using a novel method to produce printable resins, semi-IPN PAA/F127/CNC hydrogels were printed *via* DLP, with high fidelity to 3D models under different CNC concentrations. PAA/F127/CNC hydrogels were dense without evidence of layer tearing. However, the addition of CNCs above 0.25 wt% introduced morphological changes due to CNC aggregation. The preservation of F127 micelles, after PAA polymerization and crosslinking, provided evidence of a supramolecular hydrogel structure. Moreover, the PAA/F127/CNC hydrogels presented composition-dependent properties, noted by the decreasing trend in Young's modulus values and to variations in the NO release kinetics from GSNO, which are possibly related to changes in water swelling behavior in the presence of CNC. In summary, the results demonstrated that the PAA/F127/CNC/GSNO hydrogels are promising candidates to develop tailored NO-releasing medical devices.

Supporting Information

Nitric oxide-releasing 3D printed poly(acrylic acid)/F127/cellulose nanocrystal hydrogels

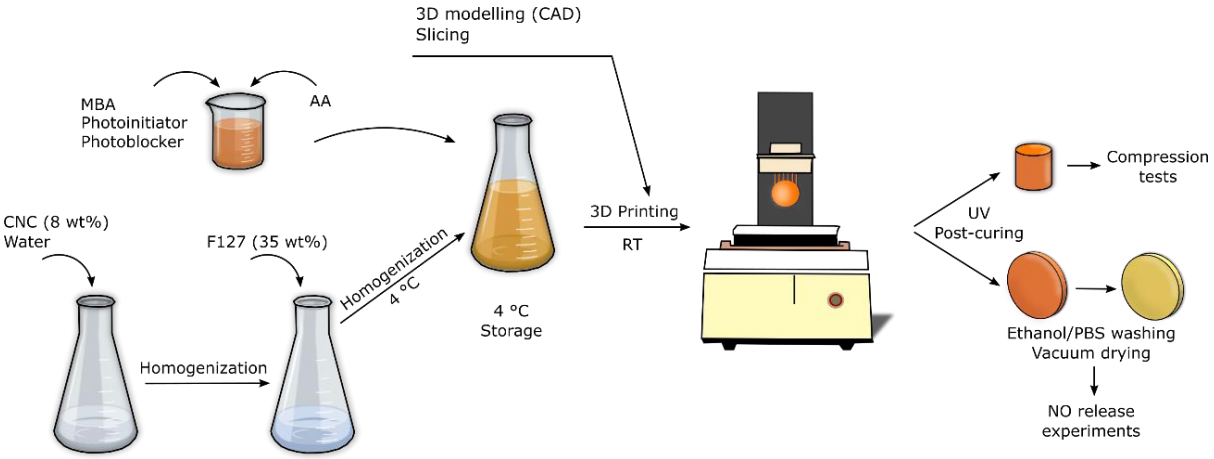

Figure S1. Scheme of the production of 3D-printable poly(acrylic acid)/ F127/cellulose nanocrystal (PAA/F127/CNC) resins and their 3D printing via DLP.

The orientation with respect to the printing head affected the object quality. **Fig. S2** shows a comparison between horizontally and vertically printed hydrogels modelled as nets (**Fig. S2A)** and their respective magnifications in **Fig. S2B** and **Fig. S2C**. The absence of voids in vertically oriented hydrogels may be due to a poorer resolution in z-axis than in the x-y plane. Consequently, in this work, hydrogels were horizontally arranged for printing, over the entire area of the printing head, as shown in **Fig. S2D** and **Fig. S2E**.

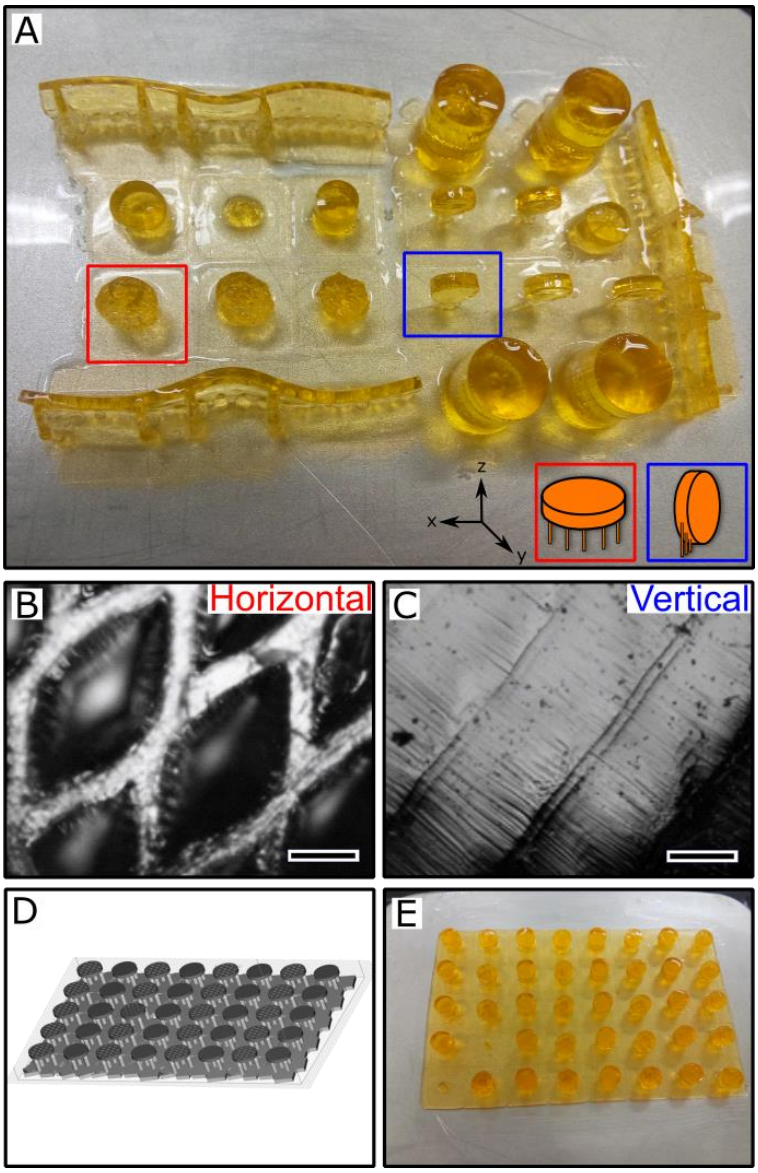

Figure S2. Effect of orientation in printing quality: (A) Horizontally (red) and vertically (blue) oriented 3D printed PAA/F127/CNC0 hydrogel nets and respective optical micrographs in (B) and (C). (D) Rendering of 3D models for printing and (E) respective hydrogels after printing process. Scale bars in (B) and (C) represent 500 µm.

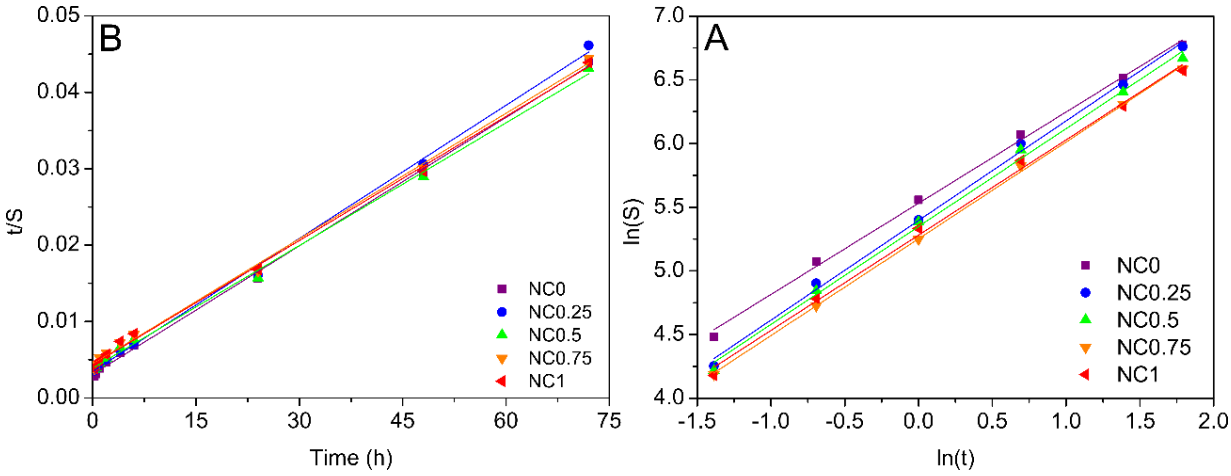

Figure S3. Kinetical study of hydrogel swelling. (A) Graphs of t/S versus time for obtention of swelling kinetic parameters from PAA/F127/CNC hydrogels. (B) Logarithmic graphs of swelling versus time during the initial 6 h of experiment for the PAA/F127/CNC hydrogels.

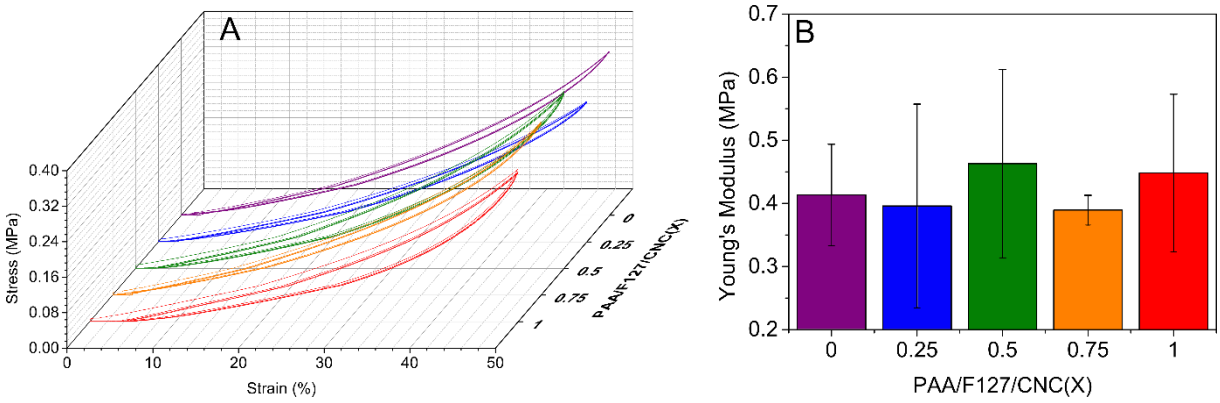

Figure S4. Compression test results of dried PAA/F127/CNC hydrogels. (A) Representative loading/unloading stress-strain curves of PAA/F127/CNC hydrogels (B) Young's Moduli as a function of CNC content.

Table S1. Kinetic parameters from linear regression of t/S vs. t plots of PAA/F127/CNC hydrogels.

Hydrogel	$(dS/dt)_0$ (g_{water} $g_{hydrogel}^{-1}$ h^{-1})	k_s (h^{-1})	S_{eq} (g_{water} $g_{hydrogel}^{-1}$)	R^2
PAA/F127/CNC0	3.23	$1.01\ 10^{-2}$	17.85	0.998
PAA/F127/CNC0.25	2.88	$9.72\ 10^{-3}$	17.23	0.998
PAA/F127/CNC0.5	2.57	$7.36\ 10^{-3}$	18.69	0.998
PAA/F127/CNC0.75	2.26	$6.77\ 10^{-3}$	18.28	0.998
PAA/F127/CNC1	2.29	$6.73\ 10^{-3}$	18.47	0.998

Table S2. Linear regression of ln S versus ln t graphs for PAA/F127/CNC hydrogels.

Hydrogel	n	k	R^2
PAA/F127/CNC0	0.72	3.62	0.997
PAA/F127/CNC0.25	0.78	2.75	0.996
PAA/F127/CNC0.5	0.77	2.63	0.996
PAA/F127/CNC0.75	0.76	2.34	0.999
PAA/F127/CNC1	0.75	2.46	0.996

Table S3. Total GSNO load for 3D printed hydrogels after impregnation with 5 mM, 10 mM and 20 mM GSNO.

	GSNO load (µmol g^{-1})	
GSNO concentration in loading solution (mM)	**PAA/F127/CNC0/GSNO**	**PAA/F127/CNC0.25/GSNO**
5	1.4±0.3	0.7±0.3
10	1.5±0.8	1.4±0.6
20	2±1	5±1

Chapter 3. Preliminary cell viability tests of PAA/F127/CNC hydrogels

Abstract

This chapter is focused on the indirect testing of PAA/F127/CNC hydrogel biocompatibility based on the viability of Vero cells. PAA/F127/CNC0 samples were extensively washed with ethanol or PBS solution prior to experiments to remove undesired residues, sterilized with ethylene oxide and then eluted in culture medium. The eluates were used in cell cultures and the cell viability was tested according to the MTT assay by Dr. Mônica Helena Monteiro do Nascimento and Prof. Amedea Barozzi Seabra from the Human and Natural Sciences Center, ABC Federal University, UFABC, Santo André, SP with a support of Felipe Nogueira Ambrosio and Prof. Christiane Bertachini Lombello from the Engineering, Modeling and Applied Social Sciences Center (CECS) installed at the UFABC.

Experimental procedure

Materials

For biological tests, Vero cells (African green monkey kidney cells) were acquired from Adolfo Lutz Institute (CCIAL 057, São Paulo – SP, BR). Ham's F10 culture medium, fetal bovine serum (FBS), phosphate buffered saline solution (PBS) and MTT (3-(4,5-dimethylthiazol-2-yl)-2,5-diphenyltetrazolium bromide) were purchased from Sigma Aldrich. Additionally, dimethyl sulfoxide (DMSO) was provided by Synth and was filtered prior to use. Prior to experiments, vacuum dried PAA/F127/CNC printed samples were extracted in ca. 500 mL ethanol or PBS solution (0.01 M, pH 7.4) for 5 days and for additional 2 days in water and the solvents were daily changed. In the sequence, hydrogels were vacuum dried for 72 h at room temperature.

Cytotoxicity Analysis

The cytotoxicity of ethanol-washed and PBS-washed 3D printed PAA/F127/CNC hydrogels was tested *in-vitro* against Vero cells, derived from African green monkey kidney cell lineages.[115,116] The cells were seeded in 96-well plates at a 1.5 10^4 cells/well density. Each well contained 100 µL of Ham's F10 medium, supplemented with 10 (wt/vol%) fetal bovine serum (FBS) and 100 µg mL^{-1} penicillin/streptomycin. Culture was maintained for 24 h at 37°C and 5 % CO_2 (COM-17AC incubator, Sanyo Scientific, Bensenville – IL, US) until a semi-confluent cell monolayer was formed.

PAA/F127/CNC hydrogel extract solutions were prepared by immersing the samples into 1 mL F10 medium for 24 h. The resulting eluates were used for an indirect cytotoxicity test, where the original culture medium was replaced by 100 µL of the extract medium. As a negative and non-cytotoxic control, cells were incubated with culture medium. For positive control of cytotoxicity, cells were exposed to a 50 v/v% DMSO solution in culture medium. After a 24 h growth period, the cell morphology was inspected in a phase-contrast light microscope (Carl Zeiss, Oberkochen – BW, DE), according to do Nascimento *et al.*[117] The MTT assay was performed for quantitative analysis of cytotoxicity, based on the procedure described by Mosmann (1983).[118] Briefly, the eluted medium was replaced by 100 µL of a 10% MTT solution (5 mg mL^{-1}) in PBS and incubated during additional 4 h. After removing the MTT solution, 50 µL of filtered DMSO were added to each well. Cell viability was then

determined by absorbance at 570 nm in an automated microplate reader (SpectraMax M5, Promega Corporation, Madison – WI, US).

Results and discussion

The cytotoxicity of printed PAA/F127/CNC0 hydrogels was tested according to an indirect testing methodology, where Vero cells were incubated with hydrogel extract solutions. This method was chosen to avoid interference of hydrogel swelling-induced alterations in cell morphology. The negative, non-cytotoxic control of Vero cells exhibited standard cell morphology and optimal conditions for culture: cells were elongated, polygonal and fibroblast-like-shaped (**Fig. 28A**). On the other hand, the positive (cytotoxic) control presented morphological alterations, due to the intrinsic DMSO cytotoxicity. In this case, a reduced number of cells in a disordered state was observed along with non-attached cells (**Fig. 28B**).

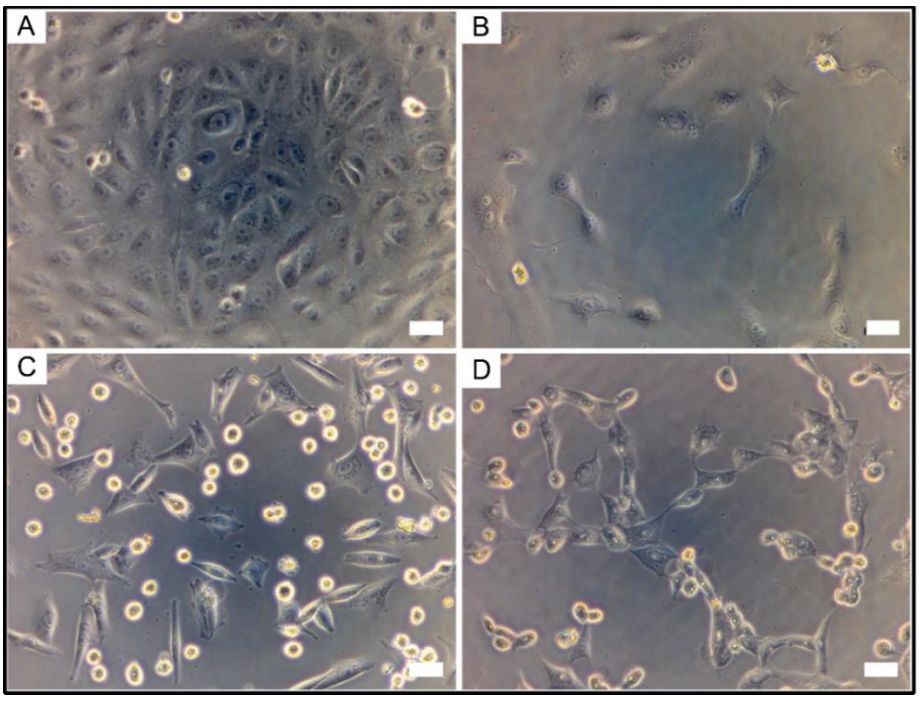

Figure 28. Micrographs of Vero cells after 24 h incubation with: (A) 10 v/v% FBS-supplemented Ham's F10 culture medium as negative control, (B) 50 v/v% DMSO in culture medium as positive control and extract medium from: (C) PBS-washed PAA/F127/CNC hydrogels and (D) ethanol-washed PAA/F127/CNC0 hydrogels. The scale bars represent 20 μm in all micrographs.

By exposing Vero cells to extract solutions, morphological alterations were observed, as shown in **Fig. 28**. PBS-washed hydrogels presented cell viability (**Fig. 28C**). However, viable cells were less numerous than the non-cytotoxic control and did not form a monolayer. In addition, suspended, round-shaped cells were observed. Similarly, ethanol-washed hydrogels (**Fig. 28D**) exhibited signs of cytotoxicity, such as a decrease in cell numbers relative to the negative control and morphological alterations, such as cell vacuolization.

MTT analysis was used to quantify cell viability, relative to the negative and positive controls (**Fig. 29**).

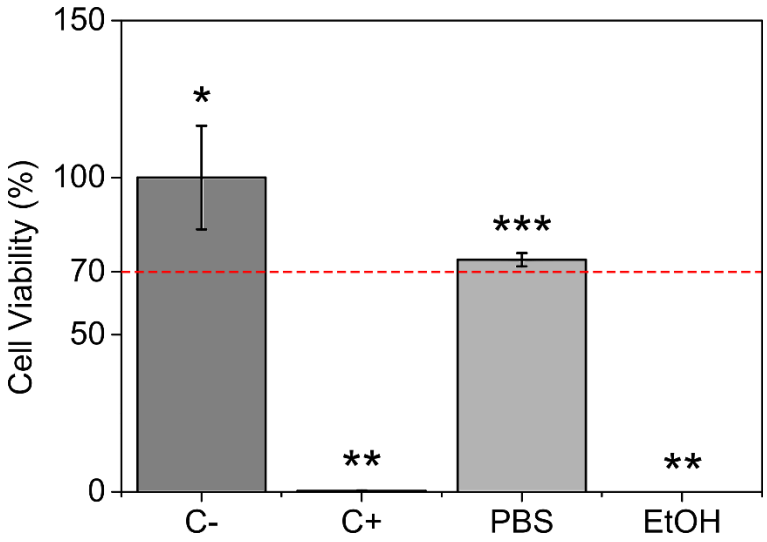

Figure 29. Vero cell viability after 24 h indirect cytotoxicity testing of extracts produced by PBS-washed and ethanol-washed PAA/F127/CNC0 hydrogel samples. Asterisk marks indicate statistical similarity for $p<0.05$: [*] represents the negative control (C-, non-cytotoxic); [**] represents the positive control (C+, cytotoxic) and the samples washed with ethanol and [***] denotes PBS-washed samples. One-way analysis of variance (ANOVA) was performed, followed by Tukey test for mean comparison.

Quantitative MTT testing supports the morphological analysis (**Fig. 28**) and shows decrease in cell viability for both tested hydrogel extracts. However, PBS-washed PAA/F127/CNC0 samples exhibited viability values that exceeded 70% with respect to the negative control, which is regarded as a limit of non-cytotoxicity.[116] Ethanol-washed

hydrogels resulted in low cell viability, regarded as a positive, cytotoxic result. A possible explanation to the influence of washing method in the cellular response relates to the neutralization of the hydrogel network. In the presence of PBS, a sodium polyacrylate network is formed, which is characterized by intense water uptake and volume increase. Therefore, swelling helps to remove residues from the dense hydrogel structure, such as monomer and initiator non-consumed during photopolymerization. Despite their high solubility in ethanol, these residues cannot be rapidly removed during ethanol washing, given the less intense swelling compared to PBS. The issue relative with the PBS washing procedure is to control the high swelling due to hydrogel neutralization, which impaired the mechanical properties of the material.

Conclusions

Preliminary indirect cytotoxicity testing of 3D printed PAA/F127/CNC hydrogels demonstrates that the application of these materials requires proper post-processing and extensive washing to remove residues. PBS washing of hydrogel samples resulted in less cytotoxic extracts than ethanol washing, apparently due to high expansion of the polymeric matrix, helping the removal of monomer and oligomer residues. Moreover, the cell viability higher than 70% exhibited by PBS washed samples indicates that the proposed printing methodology is a promising strategy to develop tissue scaffolds, expanding the available choices of printable biomaterials in further studies.

General Conclusions

The 3D printable PAA/F127/CNC hydrogel formulations were screened regarding their visual aspect and physico-chemical properties of cast and photopolymerized hydrogels. High monomer:crosslinker (AA:MBA) molar ratios resulted in flexible hydrogels, capable to retain the shapes during handling and swelling. For 3D printing, the crosslinker content in the formulations was reduced in 5x relative to the parameters obtained in the screening of photopolymerized hydrogels.

The introduction of CNCs in the 0 – 1 wt% range in the printable formulations maintained the dense hydrogel morphologies and preserved F127 micelles, however, CNC aggregates were observed in hydrogels produced in the presence of 1 wt% CNC.

A significant influence of CNCs in swelling kinetics could not be experimentally measured. However, a decrease in compressive moduli of swollen hydrogels and a modulation of the NO release profiles in GSNO-charged samples containing CNCs were observed, suggesting that CNCs modified the swelling behavior of PAA/F127/CNC hydrogels.

The NO release rates, measured by chemiluminescence, were found in the nanomolar range, which is suitable for wound healing or reduction of platelet activity applications.

PBS solution, compared to ethanol, promoted a more efficient removal of cytotoxic residues from printed hydrogels, but the intensive swelling impaired hydrogel mechanical properties and interfered in Vero cell morphology in direct cell-culture tests, requiring further studies regarding the post-processing of PAA/F127/CNC printed parts.

Future Perspectives

The exact mechanism of NO-release was not investigated in this work. Particularly, the amount of GSNO that diffuses during hydrogel rehydration could be an important parameter to be obtained, in order to determine whether the effects in a host may be local or systemic. Additionally, studies regarding the NO release for extended periods and the stability of PAA/F127/CNC/GSNO hydrogels could be addressed to investigate the long-term application and the shelf time of these materials.

The work also widens up the available strategies to obtain materials for biomedical applications, considering that alternative nanostructured systems could be introduced into the 3D printed PAA-based hydrogels in order to modulate the NO release kinetics, such as CNCs functionalized with NO-donating groups. Another perspective regarding the employed 3D printing methodology is the copolymerization of acrylic acid and acrylate-functionalized F127 in the presence of CNCs, where the covalently bound F127 micelles may act as transient crosslinks.

Lastly, referring to the biological applications of the printed PAA/F127/CNC hydrogels, it may be considered an evaluation of the intrinsic cytotoxicity of each component of the printable resins, together with the use of more friendly printing additives (photoinitiator and photoblocker) than the ones used in this work. Additionally, direct cell culture tests with human cell strains (*e. g.* fibroblasts and chondrocytes) are also recommended to endorse the application of the developed methodology to obtain implants and tissue scaffolds.

References

1. Alemán, J. V. *et al.* Definitions of terms relating to the structure and processing of sols, gels, networks, and inorganic-organic hybrid materials (IUPAC Recommendations 2007). *Pure Appl. Chem.* **79**, 1801–1829 (2007).

2. Okay, O. Hydrogel Sensors and Actuators. **6**, 1–15 (2010).

3. Lejcuś, K., Śpitalniak, M. & Dabrowska, J. Swelling behaviour of superabsorbent polymers for soil amendment under different loads. *Polymers (Basel).* **10**, (2018).

4. Peppas, N. A., Hilt, J. Z., Khademhosseini, A. & Langer, R. Hydrogels in biology and medicine: From molecular principles to bionanotechnology. *Adv. Mater.* **18**, 1345–1360 (2006).

5. McLaughlin, K. W., Wyffels, N. K., Jentz, A. B. & Keenan, M. V. The gelation of poly(vinyl alcohol) with Na2B4O7·10H2O-killing slime. *J. Chem. Educ.* **74**, 97–99 (1997).

6. Sun, J.-Y. *et al.* Highly stretchable and tough hydrogels. *Nature* **489**, 133–136 (2012).

7. Yang, T. *Mechanical and Swelling properties of Hydrogels*. *Wiley* (2012).

8. Park, H. & Robinson, J. R. Mechanisms of Mucoadhesion of Poly(acrylic Acid) Hydrogels. *Pharm. Res. An Off. J. Am. Assoc. Pharm. Sci.* **4**, 457–464 (1987).

9. Martens, P. J., Bryant, S. J. & Anseth, K. S. Tailoring the degradation of hydrogels formed from multivinyl poly(ethlene glycol) and poly(vinyl alcohol) macromers for cartilage tissue engineering. *Biomacromolecules* **4**, 283–292 (2003).

10. Baskan, T., Tuncaboylu, D. C. & Okay, O. Tough interpenetrating Pluronic F127/polyacrylic acid hydrogels. *Polymer (Guildf).* **54**, 2979–2987 (2013).

11. Bahram, M., Mohseni, N. & Moghtader, M. An Introduction to Hydrogels and Some Recent Applications. in *Emerging Concepts in Analysis and Applications of Hydrogels* (ed. Majee, S. B.) 9–38 (IntechOpen, 2016).

12. Lin, H. R. *et al.* High strain-rate response of injectable PAA hydrogel. *J. Biomater. Sci. Polym. Ed.* **26**, 534–544 (2015).

13. Lubrizol. Neutralizing Carbopol® and Pemulen Polymers in Aqueous and Hydroalcoholic Systems - Technical Data Sheets. vol. TDS-237 1–3 (2010).

14. Halacheva, S. S. *et al.* Injectable biocompatible and biodegradable pH-responsive hollow particle gels containing poly(acrylic acid): The effect of copolymer composition on gel

properties. *Biomacromolecules* **15**, 1814–1827 (2014).

15. Choi, J., Kung, H. J., MacIas, C. E. & Muratoglu, O. K. Highly lubricious poly(vinyl alcohol)-poly(acrylic acid) hydrogels. *J. Biomed. Mater. Res. - Part B Appl. Biomater.* **100 B**, 524–532 (2012).

16. Meng, Q., Peng, B. & Shen, C. Synthesis of F127/PAA hydrogels for removal of heavy metal ions from organic wastewater. *Colloids Surfaces B Biointerfaces* **167**, 176–182 (2018).

17. Jing, Z. *et al.* Biodegradable poly(acrylic acid-co-acrylamide)/ poly(vinyl alcohol) double network hydrogels with tunable mechanics and high self-healing performance. *Polymers (Basel).* **11**, (2019).

18. Tozzi, G., De Mori, A., Oliveira, A. & Roldo, M. Composite hydrogels for bone regeneration. *Materials (Basel).* **9**, 1–24 (2016).

19. Yaung, J. J. & Kwei, T. K. pH-sensitive hydrogels based on polyvinylpyrrolidone–polyacrylic acid (PVP–PAA) semi-interpenetrating networks (semi-IPN): Swelling and controlled release. *J. Appl. Polym. Sci.* **69**, 921–930 (1998).

20. Lim, L., Rosli, N., Ahmad, I., Mat Lazim, A. & Mohd Amin, M. Synthesis and Swelling Behavior of pH-Sensitive Semi-IPN Superabsorbent Hydrogels Based on Poly(acrylic acid) Reinforced with Cellulose Nanocrystals. *Nanomaterials* **7**, 399 (2017).

21. Zheng, Y. & Wang, A. Removal of heavy metals using polyvinyl alcohol semi-IPN poly(acrylic acid)/tourmaline composite optimized with response surface methodology. *Chem. Eng. J.* **162**, 186–193 (2010).

22. Shirwaiker, R. A., Purser, M. F. & Wysk, R. A. Scaffolding hydrogels for rapid prototyping based tissue engineering. in *Rapid Prototyping of Biomaterials: Principles and Applications* 176–200 (Woodhead Publishing Limited, 2014).

23. Wanka, G., Hoffmann, H. & Ulbricht, W. Phase Diagrams and Aggregation Behavior of Poly(oxyethylene)-Poly(oxypropylene)-Poly(oxyethylene) Triblock Copolymers in Aqueous Solutions. *Macromolecules* **27**, 4145–4159 (1994).

24. Mortensen, K., Batsberg, W., Hvidt, S. & Talmon, Y. Effects of PEO−PPO Diblock Impurities on the Cubic Structure of Aqueous PEO−PPO−PEO Pluronics Micelles: fcc and bcc Ordered Structures in F127. *Macromolecules* **41**, 1720–1727 (2008).

25. Jang, H. S., Kim, T. H., Do, C., Lee, M. J. & Choi, S. M. Single-walled carbon nanotube induced re-entrant hexagonal phases in a Pluronic block copolymer system. *Soft Matter* **9**, 3050–3056 (2013).

26. Schmolka, I. R. Artificial skin I. Preparation and properties of pluronic F-127 gels for treatment of burns. *J. Biomed. Mater. Res.* **6**, 571–582 (1972).

27. Yogev, S., Shabtay-Orbach, A., Nyska, A. & Mizrahi, B. Local Toxicity of Topically Administrated Thermoresponsive Systems: In Vitro Studies with In Vivo Correlation. *Toxicol. Pathol.* **47**, 426–432 (2019).

28. Basak, R. & Bandyopadhyay, R. Encapsulation of hydrophobic drugs in pluronic F127 micelles: Effects of drug hydrophobicity, solution temperature, and pH. *Langmuir* **29**, 4350–4356 (2013).

29. FDA. PMA P110003: FDA Summary of Safety and Effectiveness Data. (2011).

30. Champeau, M. *et al.* Supramolecular poly(acrylic acid)/F127 hydrogel with hydration-controlled nitric oxide release for enhancing wound healing. *Acta Biomater.* **74**, 312–325 (2018).

31. Nascimento, D. M. *et al.* Nanocellulose nanocomposite hydrogels: Technological and environmental issues. *Green Chem.* **20**, 2428–2448 (2018).

32. de Azeredo, H. M. C., Rosa, M. F. & Figueirêdo, M. C. B. Lignocellulosic-Based Nanostructures and Their Use in Food Packaging. in *Nanomaterials for Food Packaging* 47–69 (Elsevier Inc., 2018).

33. Kargarzadeh, H. *et al.* Advances in cellulose nanomaterials. *Cellulose* **25**, 2151–2189 (2018).

34. De France, K. J., Hoare, T. & Cranston, E. D. Review of Hydrogels and Aerogels Containing Nanocellulose. *Chem. Mater.* **29**, 4609–4631 (2017).

35. Martin-Martinez, F. J. Designing nanocellulose materials from the molecular scale. *Proc. Natl. Acad. Sci.* **115**, 7174 LP – 7175 (2018).

36. Brinkmann, A. *et al.* Correlating Cellulose Nanocrystal Particle Size and Surface Area. *Langmuir* **32**, 6105–6114 (2016).

37. Bajpai, S. K., Pathak, V., Chand, N. & Soni, B. Cellulose nano whiskers (CNWs) loaded-poly(sodium acrylate) hydrogels. Part-I. Effect of low concentration of CNWs on water uptake. *J. Macromol. Sci. Part A Pure Appl. Chem.* **50**, 466–477 (2013).

38. Jayaramudu, T., Ko, H. U., Kim, H. C., Kim, J. W. & Kim, J. Swelling behavior of polyacrylamide-cellulose nanocrystal hydrogels: Swelling kinetics, temperature, and pH effects. *Materials (Basel).* **12**, (2019).

39. Parker, R. M. *et al.* The Self-Assembly of Cellulose Nanocrystals: Hierarchical Design of

Visual Appearance. *Adv. Mater.* **30**, (2018).

40. Yang, J. *et al.* Studies on the properties and formation mechanism of flexible nanocomposite hydrogels from cellulose nanocrystals and poly(acrylic acid). *J. Mater. Chem.* **22**, 22467 (2012).

41. Yang, X., Bakaic, E., Hoare, T. & Cranston, E. D. Injectable Polysaccharide Hydrogels Reinforced with Cellulose Nanocrystals: Morphology, Rheology, Degradation, and Cytotoxicity. *Biomacromolecules* **14**, 4447–4455 (2013).

42. Fotie, G. *et al.* The effect of moisture on cellulose nanocrystals intended as a high gas barrier coating on flexible packaging materials. *Polymers (Basel).* **9**, 1–16 (2017).

43. Hull, C. W. Apparatus for Production of Three-dimensional Objects by Stereolithography US Patent 4,575,330. 1–16 (1984).

44. Derakhshanfar, S. *et al.* 3D bioprinting for biomedical devices and tissue engineering: A review of recent trends and advances. *Bioact. Mater.* **3**, 144–156 (2018).

45. Singh, R. & Chhabra, M. Three-Dimensional Printing. in *Reference Module in Materials Science and Materials Engineering* 1–21 (Elsevier Inc., 2017).

46. Ligon, S. C., Liska, R., Stampfl, J., Gurr, M. & Mülhaupt, R. Polymers for 3D Printing and Customized Additive Manufacturing. *Chem. Rev.* **117**, 10212–10290 (2017).

47. Guo, Y., Patanwala, H. S., Bognet, B. & Ma, A. W. K. Inkjet and inkjet-based 3D printing: Connecting fluid properties and printing performance. *Rapid Prototyp. J.* **23**, 562–576 (2017).

48. Negro, A., Cherbuin, T. & Lutolf, M. P. 3D Inkjet Printing of Complex, Cell-Laden Hydrogel Structures. *Sci. Rep.* **8**, 1–9 (2018).

49. Ilkhanizadeh, S., Teixeira, A. I. & Hermanson, O. Inkjet printing of macromolecules on hydrogels to steer neural stem cell differentiation. *Biomaterials* **28**, 3936–3943 (2007).

50. Yang, F., Tadepalli, V. & Wiley, B. J. 3D Printing of a Double Network Hydrogel with a Compression Strength and Elastic Modulus Greater than those of Cartilage. *ACS Biomater. Sci. Eng.* **3**, 863–869 (2017).

51. Chen, Z. *et al.* 3D Printing of Multifunctional Hydrogels. **29**, 1–8 (2019).

52. Tan, Z., Parisi, C., Di Silvio, L., Dini, D. & Forte, A. E. Cryogenic 3D Printing of Super Soft Hydrogels. *Sci. Rep.* **7**, 16293 (2017).

53. Bagheri, A. & Jin, J. Photopolymerization in 3D Printing. *ACS Appl. Polym. Mater.* **1**, 593–611

(2019).

54. Dutta, S. & Cohn, D. Temperature and pH responsive 3D printed scaffolds. *J. Mater. Chem. B* **5**, 9514–9521 (2017).

55. Yin, M. J. *et al.* Rapid 3D Patterning of Poly(acrylic acid) Ionic Hydrogel for Miniature pH Sensors. *Adv. Mater.* **28**, 1394–1399 (2016).

56. Gong, H., Woolley, A. T. & Nordin, G. P. High density 3D printed microfluidic valves, pumps, and multiplexers. *Lab Chip* **16**, 2450–2458 (2016).

57. Dean, D. *et al.* Multiple initiators and dyes for continuous Digital Light Processing (cDLP) additive manufacture of resorbable bone tissue engineering scaffolds. *Virtual Phys. Prototyp.* **9**, 3–9 (2014).

58. Broniowska, K. A. & Hogg, N. The Chemical Biology of S-Nitrosothiols. **17**, (2012).

59. Fukuto, J. M., Cho, J. Y. & Switzer, C. H. The Chemical Properties of Nitric Oxide and Related Nitrogen Oxides. in *Nitric Oxide* 23–40 (Academic Press, 2000).

60. Witte, M. B. & Barbul, A. Role of nitric oxide in wound repair. *Am. J. Surg.* **183**, 406–412 (2002).

61. Lotz, M. The role of nitric oxide in articular cartilage damage. *Rheum. Dis. Clin. North Am.* **25**, 269–282 (1999).

62. Thomas, D. D. *et al.* The chemical biology of nitric oxide: Implications in cellular signaling. *Free Radic. Biol. Med.* **45**, 18–31 (2008).

63. Miller, M. R. & Megson, I. L. Recent developments in nitric oxide donor drugs. *Br. J. Pharmacol.* **151**, 305–321 (2009).

64. de Oliveira, M. G. S-Nitrosothiols as Platforms for Topical Nitric Oxide Delivery. *Basic Clin. Pharmacol. Toxicol.* **119**, 49–56 (2016).

65. Langford, E. J., Wainwright, R. J. & Martin, J. F. Platelet Activation in Acute Myocardial Infarction and Unstable Angina Is Inhibited by Nitric Oxide Donors. *Arterioscler. Thromb. Vasc. Biol.* **16**, 51–55 (1996).

66. Kimura, H., Ogura, T., Kurashima, Y., Weisz, A. & Esumi, H. Effects of nitric oxide donors on vascular endothelial growth factor gene induction. *Biochem. Biophys. Res. Commun.* **296**, 976–982 (2002).

67. Champeau, M., Seabra, A. B. & de Oliveira, M. G. Hydrogels for Topical Nitric Oxide

Delivery. in *Nitric Oxide Donors* 313–330 (Elsevier, 2017).

68. Marcilli, R. H. M. & De Oliveira, M. G. Nitric oxide-releasing poly(vinyl alcohol) film for increasing dermal vasodilation. *Colloids Surfaces B Biointerfaces* **116**, 643–651 (2014).

69. Amadeu, T. P., Seabra, A. B., de Oliveira, M. G. & Monte-Alto-Costa, A. Nitric Oxide Donor Improves Healing if Applied on Inflammatory and Proliferative Phase. *J. Surg. Res.* **149**, 84–93 (2008).

70. Seabra, A. B. *et al.* S-nitrosoglutathione-containing hydrogel increases dermal blood flow in streptozotocin-induced diabetic rats. *Br. J. Dermatol.* **156**, 814–818 (2007).

71. Barros, B., Scarminio, I. & Bruns, R. *Como fazer experimentos. Pesquisa e Desenvolvimento Na Ciencia e Na Indústria* (bookman, 2001).

72. Lim, L. S., Ahmada, I., Lazima, M. A. S. M. & Aminb, M. C. I. M. Chemical crosslinking of acrylic acid to form biocompatible pH sensitive hydrogel reinforced with cellulose nanocrystals (CNC). *AIP Conf. Proc.* **1614**, 366–370 (2014).

73. Fan, K. & Boggs, J. E. Rotational isomerism of acrylic acid. *J. Mol. Struct.* **157**, 31–41 (1987).

74. Todica, M., Stefan, R., Pop, C. V. & Olar, L. IR and Raman Investigation of Some Poly(acrylic) Acid Gels in Aqueous and Neutralized State. *Acta Phys. Pol. A* **128**, 128–135 (2015).

75. Reddy, B. V. & Rao, G. R. Vibrational spectra and modified valence force field for N,N'-methylenebisacrylamide. *Indian J. Pure Appl. Phys.* **46**, 611–616 (2008).

76. Karolewicz, B. *et al.* Thermal, spectroscopic, and dissolution studies of ketoconazole-Pluronic F127 system. *J. Therm. Anal. Calorim.* **115**, 2487–2493 (2014).

77. Andhariya, N., Chudasama, B., Mehta, R. V. & Upadhyay, R. V. Biodegradable thermoresponsive polymeric magnetic nanoparticles: A new drug delivery platform for doxorubicin. *J. Nanoparticle Res.* **13**, 1677–1688 (2011).

78. Wulandari, W. T., Rochliadi, A. & Arcana, I. M. Nanocellulose prepared by acid hydrolysis of isolated cellulose from sugarcane bagasse. *IOP Conf. Ser. Mater. Sci. Eng.* **107**, (2016).

79. Lo, Y.-L., Hsu, C.-Y. & Lin, H.-R. pH-and thermo-sensitive pluronic/poly(acrylic acid) in situ hydrogels for sustained release of an anticancer drug. *J. Drug Target.* **21**, 54–66 (2013).

80. Harwood, J. A. C. & Payne, A. R. Hysteresis and strength of rubbers. *J. Appl. Polym. Sci.* **12**, 889–901 (1968).

81. Li, J., Liu, H., Wang, C. & Huang, G. A facile method to fabricate hybrid hydrogels with mechanical toughness using a novel multifunctional cross-linker. *RSC Adv.* **7**, 35311–35319 (2017).

82. Pu, X. *et al.* Ultrastretchable, transparent triboelectric nanogenerator as electronic skin for biomechanical energy harvesting and tactile sensing. *Sci. Adv.* **3**, 1–10 (2017).

83. Urrios, A. *et al.* 3D-printing of transparent bio-microfluidic devices in PEG-DA. *Lab Chip* **16**, 2287–2294 (2017).

84. Kim, Y. T., Bohjanen, S., Bhattacharjee, N. & Folch, A. Partitioning of hydrogels in 3D-printed microchannels. *Lab Chip* **19**, 3086–3093 (2019).

85. Leppiniemi, J. *et al.* 3D-Printable Bioactivated Nanocellulose-Alginate Hydrogels. *ACS Appl. Mater. Interfaces* **9**, 21959–21970 (2017).

86. Benjamin, A. D. *et al.* Light-based 3D printing of hydrogels with high-resolution channels. *Biomed. Phys. Eng. Express* **5**, 025035 (2019).

87. Teo, M. Y., Stuart, L., Aw, K. C. & Stringer, J. Micro-reactive Inkjet Printing of Three-Dimensional Hydrogel Structures. *MRS Adv.* **3**, 1575–1581 (2018).

88. Warner, J., Soman, P., Zhu, W., Tom, M. & Chen, S. Design and 3D Printing of Hydrogel Scaffolds with Fractal Geometries. *ACS Biomater. Sci. Eng.* **2**, 1763–1770 (2016).

89. Kim, K. *et al.* Lithographic resolution enhancement of a maskless lithography system based on a wobulation technique for flow lithography. *Appl. Phys. Lett.* **109**, 234101 (2016).

90. Nishikawa, M., Onuki, Y., Isowa, K. & Takayama, K. Formulation Optimization of an Indomethacin-Containing Photocrosslinked Polyacrylic Acid Hydrogel as an Anti-inflammatory Patch. *AAPS PharmSciTech* **9**, 1038–1045 (2008).

91. Naficy, S., Kawakami, S., Sadegholvaad, S., Wakisaka, M. & Spinks, G. M. Mechanical properties of interpenetrating polymer network hydrogels based on hybrid ionically and covalently crosslinked networks. *J. Appl. Polym. Sci.* **130**, 2504–2513 (2013).

92. Viana, T. N., Titotto, S. L. M. C. & Ferreira, M. J. G. C. F. 3D printing of tough supramolecular hydrogel with a low-cost home-built printer. in *XVII B-MRS Proceedings* 1284–1285 (2018). doi:978-85-63273-38-3.

93. Viana, T. N., Heinze, D. A., Titotto, S. L. M. C. & Mathilde, J. G. C. F. Otimização de hidrogel de ácido acrílico/F127 para impressão 3D: Um estudo reológico. in *Anais do 15º Congresso Brasileiro de Polímeros (15 CBPOL)* 4419–4423 (2019).

94. Lee, W. J., Clancy, A. J., Kontturi, E., Bismarck, A. & Shaffer, M. S. P. Strong and Stiff: High-Performance Cellulose Nanocrystal/Poly(vinyl alcohol) Composite Fibers. *ACS Appl. Mater. Interfaces* **8**, 31500–31504 (2016).

95. Georgii, J. L., Amadeu, T. P., Seabra, A. B., de Oliveira, M. G. & Monte-Alto-Costa, A. Topical S-nitrosoglutathione-releasing hydrogel improves healing of rat ischaemic wounds. *J. Tissue Eng. Regen. Med.* **5**, 612–619 (2011).

96. Ignarro, L. J. Nitric Oxide: A Unique Endogenous Signaling Molecule in Vascular Biology. *Biosci. Rep.* **19**, 51–71 (1999).

97. Kabirian, F. *et al.* Controlled NO-Release from 3D-Printed Small-Diameter Vascular Grafts Prevents Platelet Activation and Bacterial Infectivity. *ACS Biomater. Sci. Eng.* **5**, 2284–2296 (2019).

98. Schott, H. Kinetics of Swelling of Polymers and Their Gels. *J. Pharm. Sci.* **81**, 1990–1993 (1992).

99. Shishido, S. M., Seabra, A. B., Loh, W. & Ganzarolli de Oliveira, M. Thermal and photochemical nitric oxide release from S-nitrosothiols incorporated in Pluronic F127 gel: potential uses for local and controlled nitric oxide release. *Biomaterials* **24**, 3543–3553 (2003).

100. de Souza, G. F. P. & de Oliveira, M. G. Intratablet S-nitrosation: A New Approach for the Oral Administration of S-nitrosothiols as Nitric Oxide Donors. *J. Pharm. Sci.* **105**, 359–361 (2016).

101. Jung, Y. seok, Park, W., Park, H., Lee, D.-K. K. & Na, K. Thermo-sensitive injectable hydrogel based on the physical mixing of hyaluronic acid and Pluronic F-127 for sustained NSAID delivery. *Carbohydr. Polym.* **156**, 403–408 (2017).

102. Nikolaeva, A. L. *et al.* Nano-carbon in a hydrogel matrix for nonlinear optical applications. *Opt. Mater. (Amst).* **66**, 338–343 (2017).

103. Pappas, S. P. & Dakota, N. Photocrosslinking. in *Comprehensive Polymer Science and Supplements* (eds. Allen, G. & Bevington, J. C. B. T.-C. P. S. and S.) vol. 4 135–148 (Elsevier, 1989).

104. Mortensen, K. & Talmon, Y. Cryo-TEM and SANS Microstructural Study of Pluronic Polymer Solutions. *Macromolecules* **28**, 8829–8834 (1995).

105. Ivanova, R., Lindman, B. & Alexandridis, P. Effect of Pharmaceutically Acceptable Glycols on the Stability of the Liquid Crystalline Gels Formed by Poloxamer 407 in Water. *J. Colloid Interface Sci.* **252**, 226–235 (2002).

106. Forney, B. S., Baguenard, C. & Allan Guymon, C. Improved stimuli-response and mechanical properties of nanostructured poly(N-isopropylacrylamide-co-dimethylsiloxane) hydrogels generated through photopolymerization in lyotropic liquid crystal templates. *Soft Matter* **9**, 7458–7467 (2013).

107. Cheng, D. *et al.* Adsorption of polyethylene glycol (PEG) onto cellulose nano-crystals to improve its dispersity. *Carbohydr. Polym.* **123**, 157–163 (2015).

108. Holback, H., Yeo, Y. & Park, K. Hydrogel swelling behavior and its biomedical applications. in *Biomedical Hydrogels: Biochemistry, Manufacture and Medical Applications* (ed. Rimmer, S.) 3–24 (Woodhead Publishing Limited, 2011).

109. Işık, B. Swelling Behavior and Determination of Diffusion Characteristics of Acrylamide – Acrylic Acid Hydrogels. *J. Appl. Polym. Sci.* **91**, 1289–1293 (2004).

110. Lee, P. I. Kinetics of drug release from hydrogel matrices. *J. Control. Release* **2**, 277–288 (1985).

111. Gaharwar, A. K., Dammu, S. A., Canter, J. M., Wu, C. & Schmidt, G. Highly Extensible, Tough, and Elastomeric Nanocomposite Hydrogels from Poly(ethylene glycol) and Hydroxyapatite Nanoparticles. *Biomacromolecules* **12**, 1641–1650 (2011).

112. Chen, E. J., Novakofski, J., Jenkins, W. K. & O'Brien, W. D. Young's modulus measurements of soft tissues with application to elasticity imaging. *IEEE Trans. Ultrason. Ferroelectr. Freq. Control* **43**, 191–194 (1996).

113. Lai, Y.-S. *et al.* The Effect of Graft Strength on Knee Laxity and Graft In-Situ Forces after Posterior Cruciate Ligament Reconstruction. *PLoS One* **10**, e0127293 (2015).

114. Hodge, R. M., Bastow, T. J., Edward, G. H., Simon, G. P. & Hill, A. J. Free volume and the mechanism of plasticization in water-swollen poly(vinyl alcohol). *Macromolecules* **29**, 8137–8143 (1996).

115. Ammerman, N. C., Beier-Sexton, M. & Azad, A. F. Growth and maintenance of vero cell lines. in *Current Protocols in Microbiology* A.4E.1-A.4E.7 (John Wiley & Sons Inc, 2008).

116. ISO. *ISO 10993-5:2009(E) Biological evaluation of medical devices - Part 5: Tests for in vitro cytotoxicity*. 1–34 (2009).

117. do Nascimento, M. H. M., Ferreira, M., Malmonge, S. M. & Lombello, C. B. Evaluation of cell interaction with polymeric biomaterials based on hyaluronic acid and chitosan. *J. Mater. Sci. Mater. Med.* **28**, (2017).

118. Mosmann, T. Rapid colorimetric assay for cellular growth and survival: Application to proliferation and cytotoxicity assays. *J. Immunol. Methods* **65**, 55–63 (1983).